Article

Not peer-reviewed version

# N-Alkyl-2-(2-undecyl-1H-benzimidazol-1-yl)acetamides as An-tiproliferative Agents for Invasive Breast Cancer. Design, Syn-thesis, In Vitro Activity, and Computational Studies

Abdulaziz H. Al Khzem *, Samir M. El Rayes, Ibrahim A. I. Ali, Walid Fathalla, Mansour S. Alturki, Mohamed S. Gomaa *, Nada Tawfeeq, Mohammad Sarafroz, Abdulaziz K. Al Mouslem, Ahmed S. Alnaim, Moustafa Sarhan, Feihad Y. Alhamyani, Thankhoe A Rants'o

Posted Date: 18 February 2025

doi: 10.20944/preprints202502.1264.v1

Keywords: Benzimidazoles; breast cancer; antiproliferative activity; Molecular dynamics; lipophilicity.

 doi:10.20944/preprints202502.1264.v1



*Article*

# *N*-Alkyl-2-(2-undecyl-1*H*-benzimidazol-1-yl)acetamides as Antiproliferative Agents for Invasive Breast Cancer. Design, Synthesis, *In Vitro* Activity, and Computational Studies

**Abdulaziz H. Al Khzem [1,*], S. M. El Rayes [2], Ibrahim A. I. Ali [2], Walid Fathalla [3], Mansour S. Alturki [1], Mohamed S. Gomaa [1,*], Nada Tawfeeq [1], Mohammad Sarafroz [1], Abdulaziz K. Al Mouslem [4], Ahmed S. Alnaim [4], Moustafa Sarhan [5], Feihad Y. Alhamyani [6] and Thankhoe A. Rants'o [7]**

[1] Department of Pharmaceutical Chemistry, College of Clinical Pharmacy, Imam Abdulrahman Bin Faisal University, P. O. Box 1982, Dammam 31441, Eastern Province, Kingdom of Saudi Arabia. ahalkhzem@iau.edu.sa, msalturki@iau.edu.sa, msmmansour@iau.edu.sa

[2] Department of Chemistry, Faculty of Science, Suez Canal University, Ismailia, Egypt. samir_elrayes@yahoo.com, ibrahim3369@yahoo.com.

[3] Department of Basic Sciences, Faculty of Engineering, Suez Canal University, Ismailia, Egypt. walid3369@yahoo.com

[4] Department of Pharmaceutical Sciences, College of Clinical Pharmacy, King Faisal University, Al-Ahsa 31982, Kingdom Saudi Arabia.

[5] Department of Biomedical Sciences, College of Clinical Pharmacy, King Faisal University, Al-Ahsa 31982, Kingdom Saudi Arabia

[6] Department of Biomedical Sciences, College of Clinical Pharmacy, King Faisal University, Al-Ahsa 31982, Kingdom Saudi Arabia

[7] Department of Pharmacology and Toxicology, College of Pharmacy, University of Utah, Salt Lake City, UT 84112, USA. thankhoe.rantso@pharm.utah.edu

* Correspondence: ahalkhzem@iau.edu.sa, msmmansour@iau.edu.sa

**Abstract:** One of the most dangerous types of breast cancer that can spread from its original location to neighboring tissues is invasive breast cancer. Cathepsins, a group of proteolytic enzymes, has been thoroughly investigated in relation to cancer progression and has been shown to be crucial for the invasion and metastasis of breast cancer cells. A series of new *N*-alkyl-2-(2-undecyl-1*H*-benzimidazol-1-yl) acetamides were prepared from 2-(2-undecyl-1*H*-benzimidazol-1-yl)ethanhydrazide *via* azide coupling method with a variety of amines. The new compounds were designed to inhibit proliferation of breast cancer cells based on inhibition of the selectively and highly expressed cathepsin K. The compounds were tested for their antiproliferative activity on four cancer cell lines, namely, A549, MDA-MB231, MCF-7, U87, and HEK293 to elucidate their preferential activity on invasive breast cancer cells. The results showed that most compounds exerted enhanced activity against MDA-MD231 compared to other cell lines. Compounds **7h**, **7i**, **7a**, and **7j** showed the highest inhibition with $IC_{50}$s of 17, 27, 38, and 67 μg/ml respectively. Compounds **7a**, and **7j** showed the highest selectivity to MDA-MD231 in terms of degree of inhibition. Molecular docking supported the cathepsin K mediated activity where compound **7i**, the most potent compound, showed the best docking score of -7.126 with a low RMSD to the co-crystallized ligand pose. Molecular dynamics (MD) simulations demonstrated that **7i** maintained stability within the binding pocket with minimal fluctuations. The postulated lipophilicity impact on activity was evaluated through LLE calculations, where values for the most active compounds demonstrated that optimal potency was frequently associated with moderate lipophilicity, as seen in compound **7i** (LLE = 2.69). Thus, the developed compounds are promising antiproliferative agents for invasive breast cancer where a cathepsin inhibition pathway is implicated.

 doi:10.20944/preprints202502.1264.v1



**Keywords:** Benzimidazoles; breast cancer; antiproliferative activity; molecular dynamics; lipophilicity

## 1. Introduction

Invasive breast cancer is one of the most aggressive cancers, defined by its ability to spread beyond its initial location to surrounding tissues. In invasive breast cancer, the tumor cells invade the basement membrane, meaning they can invade the surrounding tissues, and the risk of metastasis is high [1]. Understanding the molecular basis of this invasiveness has revealed that lysosomal proteases, particularly the cathepsin family, are essential for cancer cell invasion and metastasis [2]. Cathepsins, a group of proteolytic enzymes, have been extensively studied in the context of cancer progression and it has been found to play an essential role in cancer development and in the invasive process.

Among cathepsins, cathepsins B, D, and L are the most well-studied cathepsins in the context of cancer invasion and metastasis. They enhance cancer progression through extracellular matrix (ECM) protein degradation, critical for tumor cell migration and invasion [3–6]. Moreover, cathepsin K is an endopeptidase which works in both lysosomal and extracellular regions [7]. It has a relatively specific role in bone remodeling and is primarily limited to osteoclasts [8]. But a preliminary study found that this protease is expressed in both primary cancer of the breast cells and bone tumors [9,10]. Crucially, cathepsin K activity is often higher in breast cancer cells, implying that this enzyme plays an important role in enabling breast cancer cells to spread to bone [7]. One biochemical method by which cathepsin K stimulates ECM breaking matrix, which leads to breast cancer cell spreading and metastatic potential [11]. Furthermore, secreted cathepsin K can degrade ECM components [12].

Research has been done on the expression of cathepsin in various breast cancer cell lines, and the results have shown that the activity of cathepsin differs. The high invasiveness of MDA-MB-231 cells is reflected in the increased activity of cathepsin compared to less invasive lines, for example, MCF-7 [13]. In hypoxic environments, cathepsin is overexpressed in MDA-MB-231 cells, increasing their migration and epithelial-to-mesenchymal transition (EMT), thus contributing to their malignant phenotype [13,14]. On the other hand, MCF-7 cells with low cathepsin levels display limited invasiveness, therefore underlining the relationship between cathepsin levels and cancer cell invasiveness.

Studying cathepsin expressions in other types of cancer also provides information about their oncogenic functions. For instance, cathepsin B is over-expressed in lung adenocarcinoma (A549), through which it promotes the invasiveness of the tumor [15]; cathepsins B and L are over-expressed in glioblastoma (U87) through which they facilitate the aggressive invasion into brain tissue [16]. On the other hand, normal cells (KEK) show relatively low cathepsin levels [17]. Such differential expression pattern further supports that cathepsins offer a selective advantage to the tumor cells over normal cells.

Since cathepsins have been observed to be overexpressed in various types of cancer, inhibiting it may be an effective cancer treatment strategy. Several cathepsin inhibitors have been investigated as potential anticancer therapeutic agents. These inhibitors prevent the degradation of ECM, and thereby decrease cancer cell invasion and metastasis [18]. A number of specific cathepsin inhibitors have shown promise, such as kaempferol, chloroquine, and Pepstatin A [4,15,19].

Moreover, the use of cathepsin inhibitors, together with other cancer treatments, has been seen to cause cumulative effects. For example, kaempferol exhibits an antiproliferative effect through the inhibition of cathepsin D. It increases the efficacy of other chemotherapeutic drugs, which may be potentially helpful for the treatment of highly malignant tumours, including breast cancer and glioblastoma [20]. These results imply that cathepsin inhibitors may have therapeutic value in cancers that overexpress cathepsin. Further studies of cathepsin inhibitors are needed to determine the effectiveness of these compounds in clinical practice and their potential synergism with other

 doi:10.20944/preprints202502.1264.v1



treatments to enhance patients' prognosis. As discussed above, cathepsin K represents a good target for breast cancer given its limited occurrence to osteoclasts under normal conditions and its overexpression in breast cancer, that would allow suitable selectivity for clinical development.

Relacatib, Balicatib, and Odanacatib, are cathepsin K inhibitors that progressed to clinical trials phases I, II, and III, respectively (Figure 1). The structures show a common feature of a peptidomimetic chain on an aromatic scaffold including phenyl, biphenyl, and benzofuran.

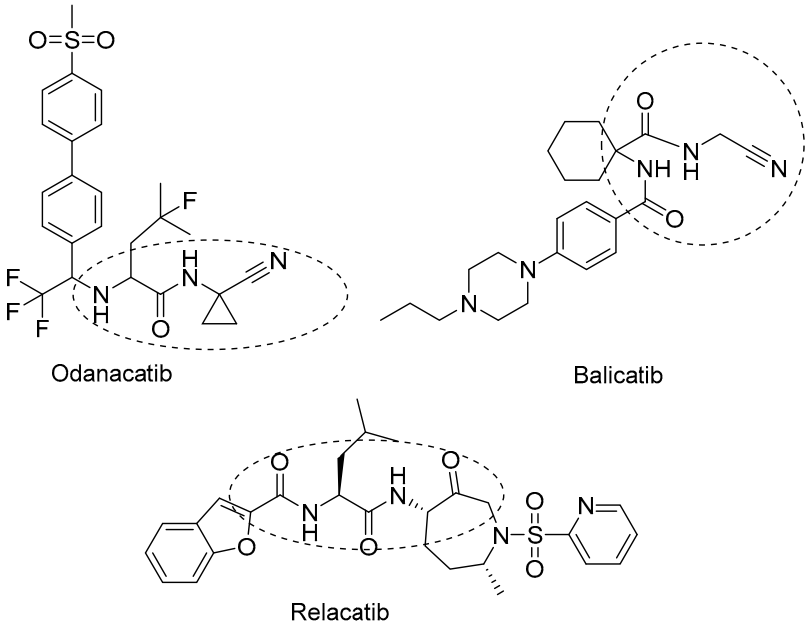


**Figure 1.** Structures of cathepsin K inhibitors with highlight in the common structural features.

Benzimidazole is an important class of biologically active compounds showing a wide range of applications in medicinal chemistry including Anti-inflammatory [21,22], Antihypertensive [23], anticancer [24–27], antioxidant [28], Anthelmintic [29,30], Antispasmodic [31] and antimicrobial activities [32–35]. Figure 1 shows the marketed drugs containing benzimidazole ring system. Benomyl [36] and Carbendazim [37] were used as antimicrobial while Pracinostat (histone deacetylase inhibitor) [38,39] and Bendamustine (chronic lymphocytic leukemia, multiple myeloma and lung cancer) were used as antitumour, (Figure 2) [40,41].

The pharmacokinetic properties are also crucial for the drug to reach its site of action and of utmost importance in case of solid tumors is penetration [42,43]. Based on that, we designed a series N-1 peptidomimetic substituted and N-2 lauryl substituted benzimmidazoles. We utilized the azide coupling method described before by our group in the structure modification of a number of heterocyclic compounds f [44–50]. This method offers the attachment of a wide range of functionalities ranging from lipophilic to hydrophilic by simple addition of a variety of amines and amino acids and amino acid esters. Herein, we report on the synthesis and characterization of N-alkyl-2-(2-undecyl-1H-benzimidazol-1-yl)acetamides and their antiproliferative activity.

 doi:10.20944/preprints202502.1264.v1



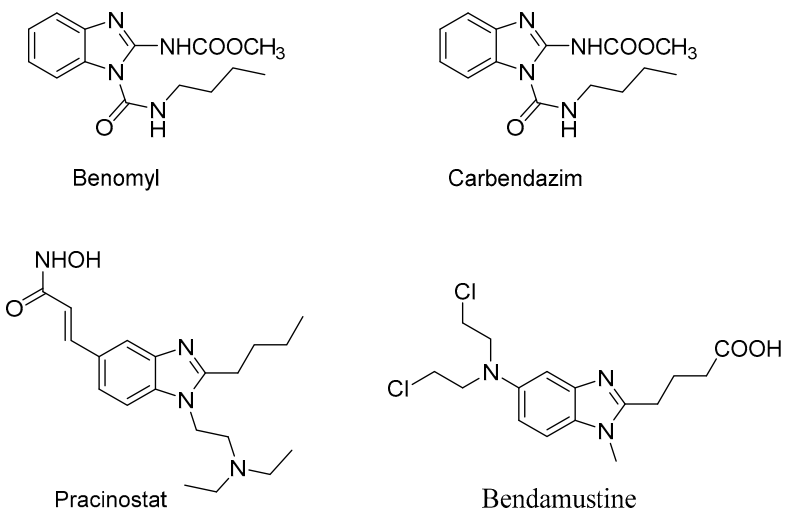


**Figure 2.** Marketed drugs containing benzimidazole ring system.

## 2. Results and Discussion

### *2.1. Compounds Design*

The structure of cathepsin K inhibitors that progressed to clinical trials revealed that they have an aromatic core scaffold substituted with a short peptidomimetic chain (Figure 3). We designed our compounds to contain benzimidazole, a privilege scaffold in drug discovery, as the core structure and substituted in position 1 with various peptidomimetic chains. We also considered the pharmacokinetic properties, especially tissue penetration in our design. Tissue penetration could be improved through various strategies. Among these strategies is the use of drug lipophilic conjugates (LCs). Alcohol or amine, glycerides, phospholipids, cholesterol, bile salts, long-chain hydrocarbons, or analogues of squalene might all be considered lipophilic residues. Lipophilic conjugates can be utilized to accomplish a range of drug delivery and pharmacokinetic advantages through a number of methods, including enhancing passive membrane permeability or significantly changing drug-transporter or drug-metabolic enzyme interactions. Furthermore, improved drug binding to endogenous lipid carriers such as albumin by lipophilic conjugation may change the way drugs are metabolized, excreted, and disposed of [51–53]. Therefore, we incorporated a long lipophilic lauric acid chain in position 2 together with the peptidomimetic structure (Figure 3).

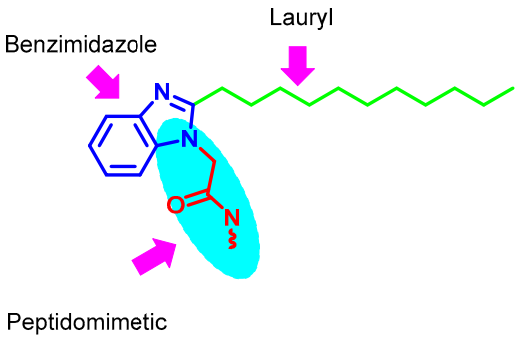


**Figure 3.** Compound design of the benzimidazole derivatives.

### *2.2. Chemical Synthesis*

The model compound 2-undecyl-1-*H*-benzimidazole was prepared by the reaction of 1,2-phenylene diamine with lauric acid under reflux condition in solvent for 4 h [54]. The structure of benzimidazole **3** with a pronounced nucleophilic character, reacted with ethylchloro acetate in acetone under reflux condition for 10 h. and gave methyl 2-(2-undecyl-1*H*-benzimidazol-1-yl) acetate

Preprints.org (www.preprints.org) | NOT PEER-REVIEWED | Posted: 18 February 2025 doi:10.20944/preprints202502.1264.v1



(**4**) in 93 % yield. The ester 4 subsequently reacted with hydrazine hydrate in ethanol for 10 h. and gave 2-(2-undecyl-1-*H*-benzimidazol-1-yl)ethanhydrazide (**5**) in 85 % yield (Scheme 1).

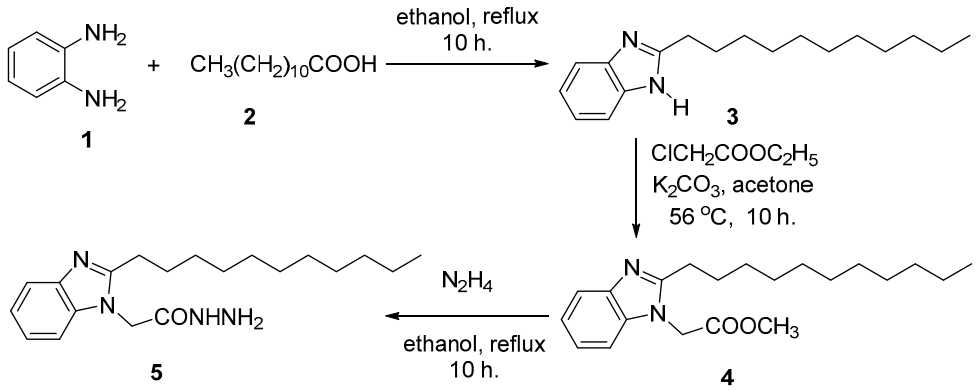


**Scheme 1.** Preparation of 2-(2-undecyl-1*H*-benzimidazol-1-yl)ethanhydrazide (**5**).

The hydrazide **5** is an excellent precursor for the structure modification of benzimidazole ring system via azide coupling method. The structure could be modified by the attachment of amine residues covering a wide range of lipophilic and hydrophilic features through a peptide bond. Thus, 2-(2-undecyl-1*H*-benzimidazol-1-yl)ethanhydrazide (**5**) reacted with sodium nitrite and HCl at low temperatures to afford the in-situ generated azide **6**, which subsequently reacted with amines: propyl amine, butyl amine, isopropyl amine, isobutyl amine, allyl amine, benzyl amine, cyclohexyl amine, diethyl amine, morpholine and piperidine to give *N*-alkyl-2-(2-undecyl-1*H*-benzimidazol-1-yl) acetamides **7a-j** in 68-89 % yield (Scheme 2).

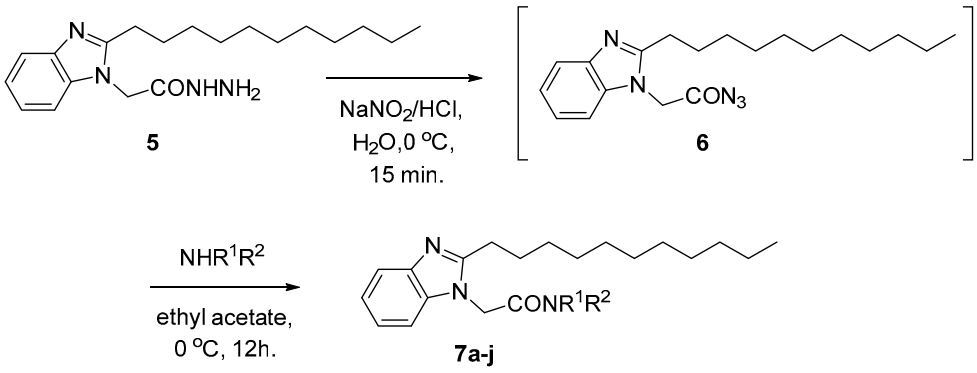


| 7 | $NR^1R^2$ | Abbrev. | 7 | $NR^1R^2$ | Abbrev. | 7 | $NR^1R^2$ | Abbrev. |
|---|---|---|---|---|---|---|---|---|
| **a** | $NH(CH_2)_2CH_3$ | propyl amine | **b** | $NH(CH_2)_3CH_3$ | butyl amine | **c** | $NHCH(CH_3)_2$ | isopropyl amine |
| **d** | $NHCH_2CH(CH_3)_2$ | isobutyl amine | **e** | $NHCH_2CH{=}CH_2$ | allyl amine | **f** | 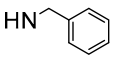 | benzyl amine |
| **g** |  | cyclohexyl amine | **h** | $N(CH_2CH_3)_2$ | diethyl amine | **i** |  | morpholine |
| **j** |  | piperidine | | | | | | |

**Scheme 2.** Preparation of *N*-alkyl-2-(2-undecyl-1*H*-benzimidazol-1-yl)acetamides **7a-j** .

The structure assignment of the 2-(2-undecyl-1H-benzimidazol-1-yl)ethanhydrazide (**5**), methyl 2-(2-undecyl-1*H*-benzimidazol-1-yl) acetate (**4**), and *N*-alkyl-2-(2-undecyl-1*H*-benzimidazol-1-yl)acetamides **7a-j** were based on $^1H$, $^{13}C$ NMR as well as physicochemical analysis.

 doi:10.20944/preprints202502.1264.v1



Thus, the $^{1}$H NMR spectrum of 1-morpholino-2-(2-undecyl-1*H*-benzimidazol-1-yl) ethan-1-one (**7i**) showed a unique NMR pattern, gave two pairs of triplet and multiplet signals at δ 2.66, 2.22, 1.49-1.56 and 1.72-1.80 ppm corresponding to two diastereotropic protons of two $CH_2$ groups (C1, C2) of the long chain lauric acid residue attached to the benzimidazole ring system. The $^{1}$H NMR spectrum of **7i** also shows two multiplet signals at 0.78-0.82 and 1.16-1.21 ppm corresponding to $CH_3$ and 8 $CH_2$ groups, respectively of lauric acid residue. The $^{1}$H NMR pattern of lauric acid residue attached to benzimiodazole was repeated in all $^{1}$H NMR of the prepared compounds **7a-j**. Finally, the $^{1}$H NMR spectrum of **7i** showed signals at 7.02-7.85 and 4.78 corresponding to four aromatic CH and NCH2CO groups, respectively. The $^{13}$C NMR spectrum of 7i showed signals at δ 41.8, 46.0, 66.7, 67.0 and 164.4 ppm corresponding to 2 $NCH_2$, $NCH_2CO$, $OCH_2$, $OCH_2$ and C=O groups, respectively.

*2.3. Antiproliferative Assay*

Ten synthesized chemical compounds were assayed for their cytotoxicity against the four human cancer cell lines (A549, MDA-MB 231, MCF-7, U87) and HEK 293.

MTT assay evaluated the effect of ten synthesized chemical compounds at different concentrations (1000 -1.0 µg/ml) on the cell viability of the four human tumour cell lines (A549, MDA-MB 231, MCF-7, U87) and on the non-tumor cell line (HEK 293), which was used as control. Cytotoxic activity of compounds **7a-7j** are shown in Figure 4. The results demonstrated that the cytotoxic activity of compounds on the tumor cell lines increased in dose-dependent manner, observed as reduced survival percentages. The highest compound concentration evaluated (1000 µg/ml) resulted in a survival of 7.0–17.0 % for different cells. When testing the 1.0 µg/ml concentration of each compound, the lowest concentration evaluated, the survival of most tumor cells achieved 100% for different cells. Similarly, when testing the 10.0 µg/ml concentration of each compound, the survival of tumor cells achieved 100% for different cells. Moreover, when testing the 100.0 µg/ml concentration of compound **7i**, the survival of tumor cells achieved 7-11% for different tumor cells while achieved 91% for normal cells. At the same concentration, (100.0 µg/ml) of compounds **7e** and **7b**, the survival of all tested cells achieved 80-100%. The survival of all tested cells achieved more than 50% in case of 100.0 µg/ml after treatment with compounds **7c** and **7d**. In case of **7a**, **7f**, **7h**, **7j**, more reduction of survival of most cells was observed at the same concentration (100.0 µg/ml). Interestingly, results showed that MDA-MB 231 was the most affected cells by several compounds **7i** (7%), **7c** (49%), **7g** (50%), **7d** (60%), **7a**, **7f**, **7h**, **7j** (10-27%).

Cells were treated with different concentrations (10-fold descending concentration; 1000 -1.0 µg/ml) of each compound. In terms of their IC50 values, it should be noted that compound **7i** showed the best inhibition profile on all four cancer cell lines (A549, MDA-MB 231, MCF-7, U87); IC50; 30, 27, 14 and 17 µg/ml respectively, with high IC50 on HEK cells (499 µg/ml). Similarly, compound 7h showed low IC50 on all tested cell lines (A549, MDA-MB 231, MCF-7, U87 and HEK); 37, 17, 37, 80 and 68 µg/ml, respectively. However, the other eight compounds did not show promising IC50 on all tested cells except compound **7a** showed IC50; 38 µg/ml on MDA-MB 231 cell line (Table 1).

It is noteworthy that most of the tested compounds, **7a**, **7c**, **7d**, **7g**, **7h**, and **7j**, showed the best inhibition on the more invasive MDA-MB231 compared to other cell lines. Compounds **7h**, **7i**, **7a**, and **7j** showed the highest inhibition with IC50s of 17, 27, 38, and 67 µg/ml respectively. While regarding cancer type selectivity, compounds **7a**, and **7j** showed the highest selectivity to MDA-MD231 in terms of degree of inhibition. It is therefore depicted that the activity of these compounds could be mediated through cathepsin inhibition which are highly expressed in the more invasive cancer types.

**Table 1.** IC50 values obtained for the synthesized chemical compounds.

| Compound | $IC_{50}$ (µg/ml) | | | |
|---|---|---|---|---|
| | **A549** | **MDA-MB 231** | **MCF7** | **U87** |
| **7a** | 661 | 38 | 120 | 95 |
| **7b** | 603 | 465 | 464 | 450 |

 doi:10.20944/preprints202502.1264.v1



| | | | | |
|---|---|---|---|---|
| **7c** | 300 | 106 | 115 | 160 |
| **7d** | 841 | 121 | 371 | 150 |
| **7e** | 555 | 421 | 484 | 300 |
| **7f** | 94 | 107 | 71 | 95 |
| **7g** | 117 | 97 | 370 | 250 |
| **7h** | 37 | 17 | 37 | 80 |
| **7i** | 30 | 27 | 14 | 17 |
| **7j** | 187 | 67 | 368 | 250 |

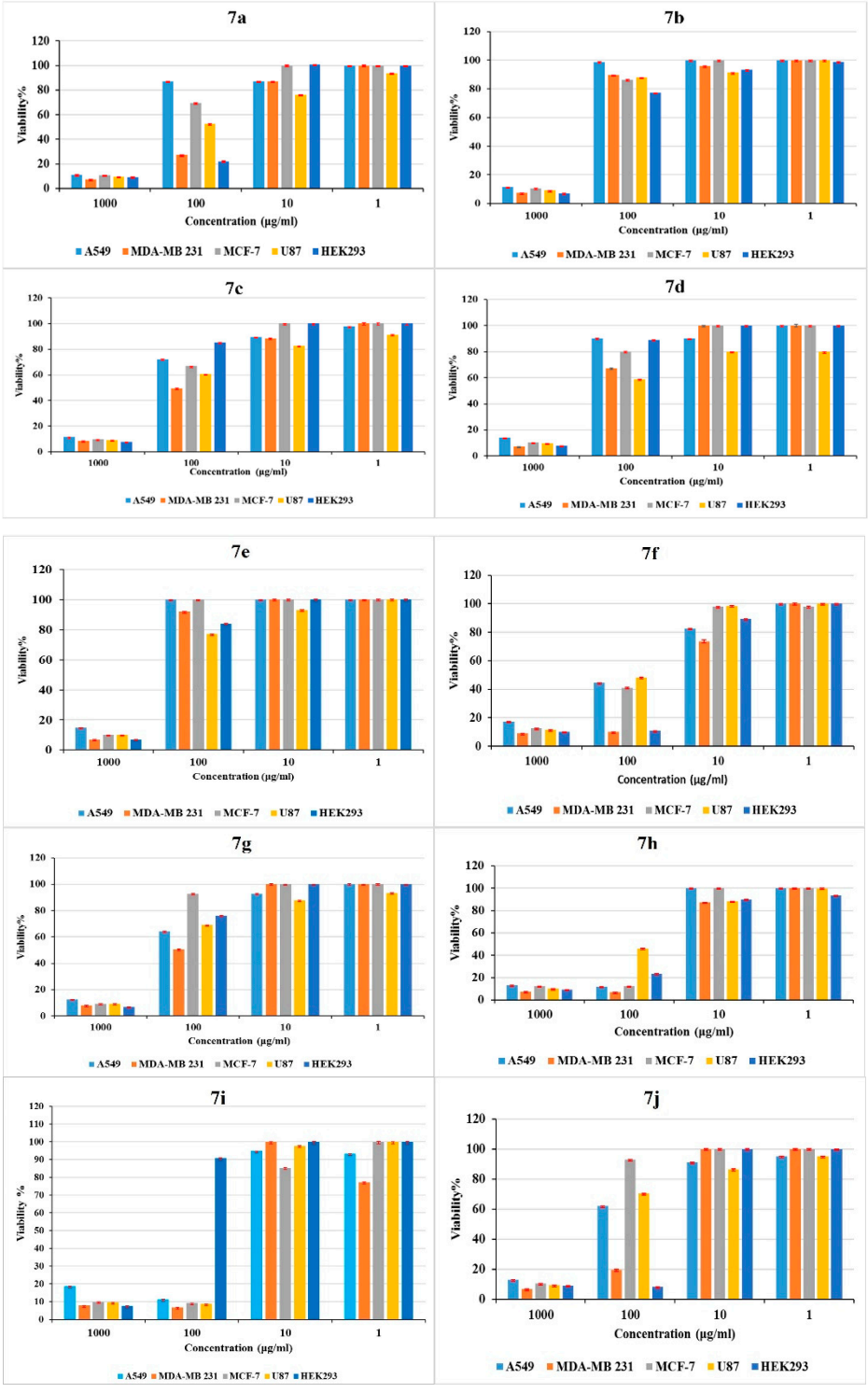

 doi:10.20944/preprints202502.1264.v1



**Figure 4.** Cell viability analysis using the MTT assay. Viability of a panel of four cancer cell lines (A549, MDA-MB231, MCF-7& U87) and a normal human embryo kidney cell line (HEK293) after treatment with compounds 7a-j at different concentrations (1000-1.0 µg/ml) for 24 h. Cell viability was shown as the percentage of DMSO control. Data were obtained from three replicates and were represented as means ± SEM (mean ± SEM).

*2.4. Ligand Lipophilic Efficiency (LLE)*

The ligand lipophilic efficiency (LLE) investigation regarding the highly potent hits **7a**, **7h**, **7i**, and **7j** displayed a clear relationship between lipophilicity as represented by clogP and the associated biological activity represented by pIC50 values. The LLE is calculated by subtracting the clogP from the pIC50, which reflects the balance between potency and lipophilicity. The clogP ranges from 4.77 to 5.63, thus giving a ligand lipophilic efficiency of 0.40 up to 2.69. For the A549 cell line, 7a has a logP of 5.41 and an pIC50 of 6.75, resulting in an LLE of 1.34, which is somewhat highly lipophilic and thus may have limited biological activity. On the contrary, compound 7i with a clogP = 4.77 showed pIC50 = 7.12 with an LLE of 2.35, indicating good lipophilicity with high potency and resulting in a more balanced profile. Compound **7j**, with a clogP value of 5.63, showed a lower LLE of 0.70, which points toward lower lipophilicity and thus may reduce its overall drug-likeness. In addition, compound 7h, which has a clogP value of 5.54, displays an LLE of 1.48, signifying reduced biological action and effectiveness. Comparable patterns were noted on the other cell lines, such as MDA-MB 231, MCF7, and U87 (Table 2).

LLE is a useful metric for balancing drug-like molecules with respect to their potency and lipophilicity. Potency is usually represented as IC50 or Ki value, a way to express the activity of a compound inhibiting any target. Similarly, lipophilicity can be given as clogP or logP, relating to the property profile in ADMET. These features are combined in LLE by subtracting clogs from pIC50 to give a holistic view of the potency of a compound. High values of LLE indicate a highly biologically active compound with moderate lipophilicity value associated with higher oral bioavailability, superior metabolic stability, and reduced off-target effects, which makes LLE an indispensable tool in active compound identification during the preclinical and clinical development stages [55,56]. LLE values for the most active compounds revealed that optimal potency often correlated with moderate lipophilicity, as observed in compound **7i**.

**Table 2.** Ligand Lipophilic Efficiency (LLE) of the compounds 7a, 7h, 7i, and 7j in the four cancer cell lines (A549, MDA-MB231, MCF-7& U87).

| | **$pIC_{50}$** | **ClogP** | **LLE1** | | **$pIC_{50}$** | **ClogP** | **LLE[1]** |
|---|---|---|---|---|---|---|---|
| Compound/ Cell line | | **A549** | | Compound/ Cell line | | **MCF7** | |
| **7a** | 6.75 | 5.41 | 1.34 | **7a** | 6.49 | 5.41 | 1.08 |
| **7h** | 7.02 | 5.54 | 1.48 | **7h** | 7.02 | 5.54 | 1.48 |
| **7i** | 7.12 | 4.77 | 2.35 | **7i** | 7.46 | 4.77 | 2.69 |
| **7j** | 6.33 | 5.63 | 0.70 | **7j** | 6.03 | 5.63 | 0.40 |
| | | **MDA-MB 231** | | | | **U87** | |
| **7a** | 6.99 | 5.41 | 1.58 | **7a** | 6.59 | 5.41 | 1.18 |
| **7h** | 7.36 | 5.54 | 1.82 | **7h** | 6.68 | 5.54 | 1.14 |
| **7i** | 7.17 | 4.77 | 2.40 | **7i** | 7.37 | 4.77 | 2.60 |
| **7j** | 6.77 | 5.63 | 1.14 | **7j** | 6.20 | 5.63 | 0.57 |

1LLE= pIC50 – clogP or D.

 doi:10.20944/preprints202502.1264.v1



*2.5. In-Silico Analysis*

2.5.1. Docking Studies Analysis

The cognate ligand was redocked back into its target cathepsin K using the same procedure and protocol applied for the ten hits to validate docking. After that, rigid-body superposition was done using Maestro's structure superposition tool by aligning the predicted lowest energy conformation of the target with its corresponding co-crystalline ligand. The root mean standard deviation (RMSD) of the predicted binding poses from the co-crystalline pose was calculated using classical RMSD, considering RMSD < 2 Å as an adequate threshold for validating correctly posed molecules, according to references [57,58]. As shown in Figure 5, the results obtained indicated good superimposition of the binding mode, represented by a value of 0.1019 Å for I10 300, exhibiting the accuracy of Glide's pose prediction.

Molecular docking was performed to investigate the binding characters of the ten hits with cathepsin K active site and their correlation with their antiproliferative activity on A549, MDA-MB231, MCF-7 and U87 cancer cell lines (Table 1). The most potent compound was **7i**, with a docking score of -7.126. The interaction of **7i** with the cathepsin K displayed that the compound is anchored in the binding pocket, with its strong interaction mainly stabilized by hydrogen bonds between the indole of **7i** and LEU-160. The oxygen atom in the morpholine ring acts as a hydrogen bond acceptor and interacts with GLY-66 to increase the selectivity of binding (Figures 6 and 7). Other weaker interactions, such as van der Waals (VDW) contribute to the overall stability of **7i**. Molecular docking is a computational method to predict how exactly the ligand interacts with the receptor by predicting the preferred orientation of a molecule in the binding site of a target protein [59].

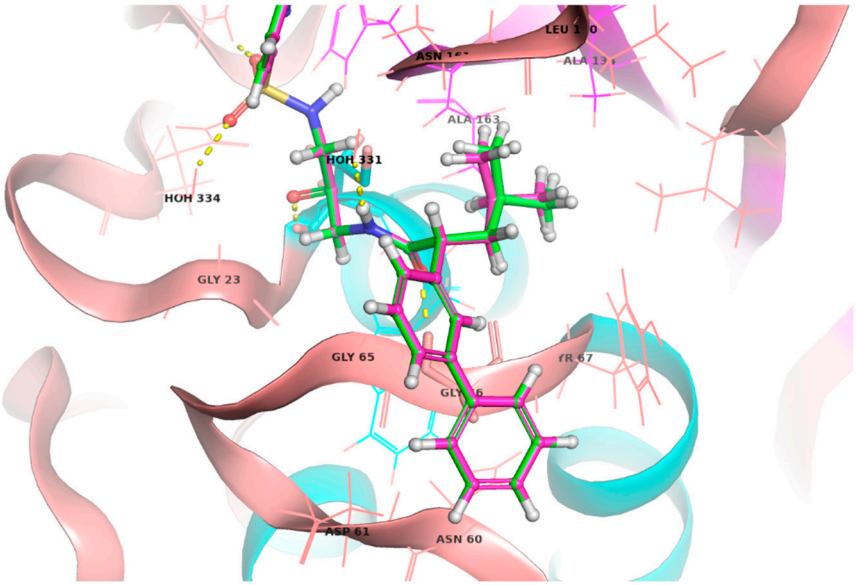


**Figure 5.** Comparison of binding poses of the co-crystal ligand (green sticks, atom color) and the redocked ligand (magenta sticks, atom color) within the cathepsin K binding site, with an RMSD of 0.1019Å.

In this study, molecular docking was used to assess the binding of the synthesized compounds to the active site of cathepsin K and their binding affinities ranked based on their glide scores. Interestingly, compound **7i** was the most potent, showing a high docking score of -7.126. It was further stabilized by hydrogen bonding contributions and favorable van der Waals interactions, maintaining stability in its binding conformation. The structural pose of **7i** inside the cathepsin K binding pocket with a low RMSD to the co-crystallized ligand further supported the accuracy of the docking simulations.

 doi:10.20944/preprints202502.1264.v1



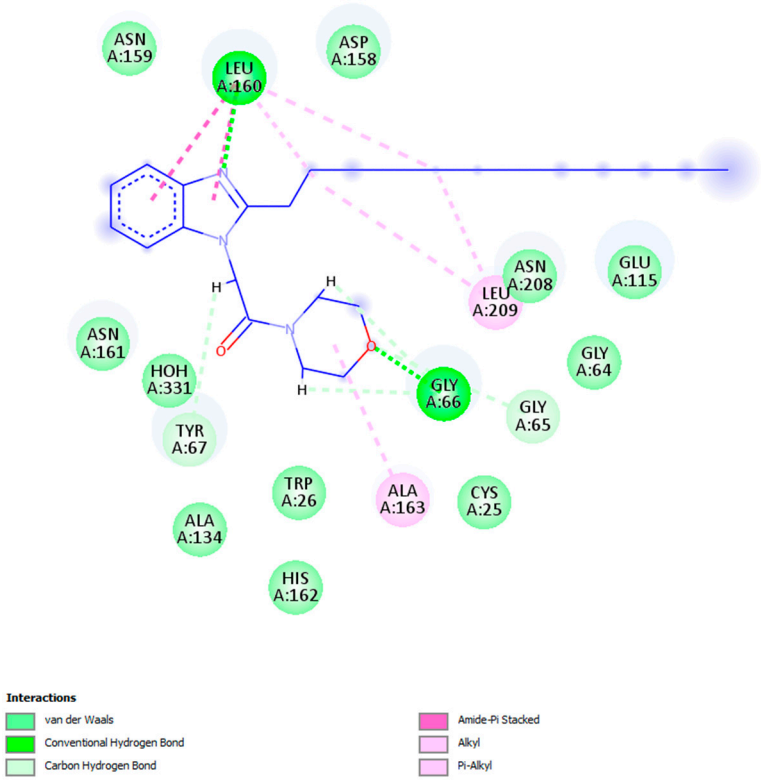


**Figure 6.** Two-dimensional ligand-protein binding interactions of cathepsin K bounded to **7i.**

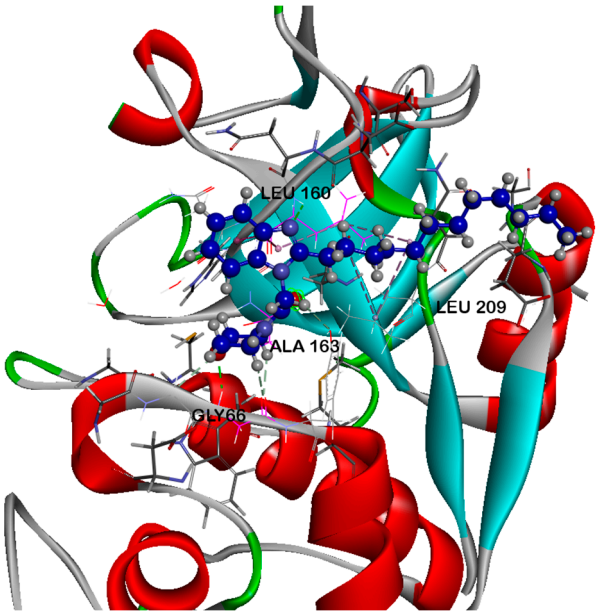


**Figure 7.** Ligand–protein binding interactions. Three-dimensional cartoon and surface representation of cathepsin K bounded to **7i** (sticks, blue color).

### 2.5.2. Molecular Dynamics (MD) Analysis

In the molecular dynamics (MD) analysis of cathepsin K-7i complex, both the ligand and receptor stayed equilibrated throughout the simulation (Figure 8). Nevertheless, there was a short occurrence of rapid fluctuations of 7i at about 85-90 ns followed by the restored equilibration. The RMSD of cathepsin K during this assessment was maintained below 2.0 while that of 7i was ~3.0. These low RMSDs suggested a highly stable complex between cathepsin K and 7i [59].

Preprints.org (www.preprints.org) | NOT PEER-REVIEWED | Posted: 18 February 2025 doi:10.20944/preprints202502.1264.v1



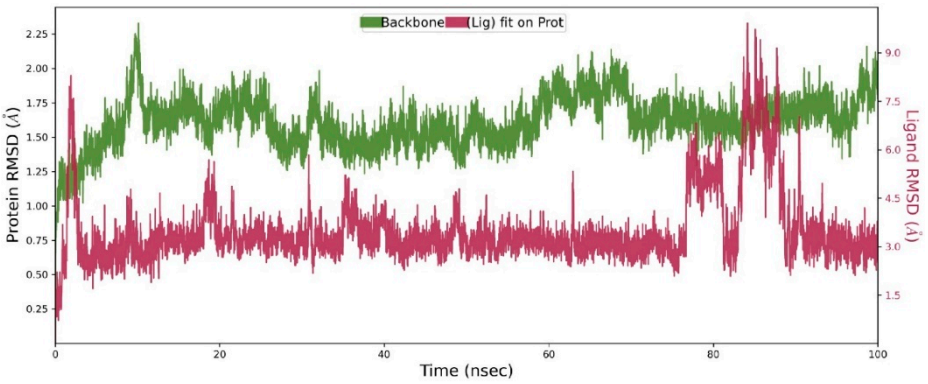


**Figure 8.** The overlaid RMSDs of cathepsin K and **7i** during the MD simulation.

In the MD calculations of cathepsin K-**7i** complex (Figure 9), the morpholine ring of **7i** was involved in hydrophobic interactions with ALA-134. In addition, the direct hydrogen bonding through GLY-66 and that mediated through the water bridge to LEU-160 were established. These positioned the **7i**'s indole ring, made of the benzene and pyrrole rings, closer to the critical aromatic residues such as TYR-67 for conformational stabilization. Thus, the major aromatic hydrophobic interaction of TYR-67 to the benzene ring as well as the water bridge-assisted hydrogen bonds between GLY-64 and ASP-61 to the pyrrole ring of **7i** were essential to stabilize the final pose. Specifically, this maintained the long alkyl side chain in a stabilized position towards the TRP-184; TRP-184 provided constant hydrophobic interactions with the side chain.

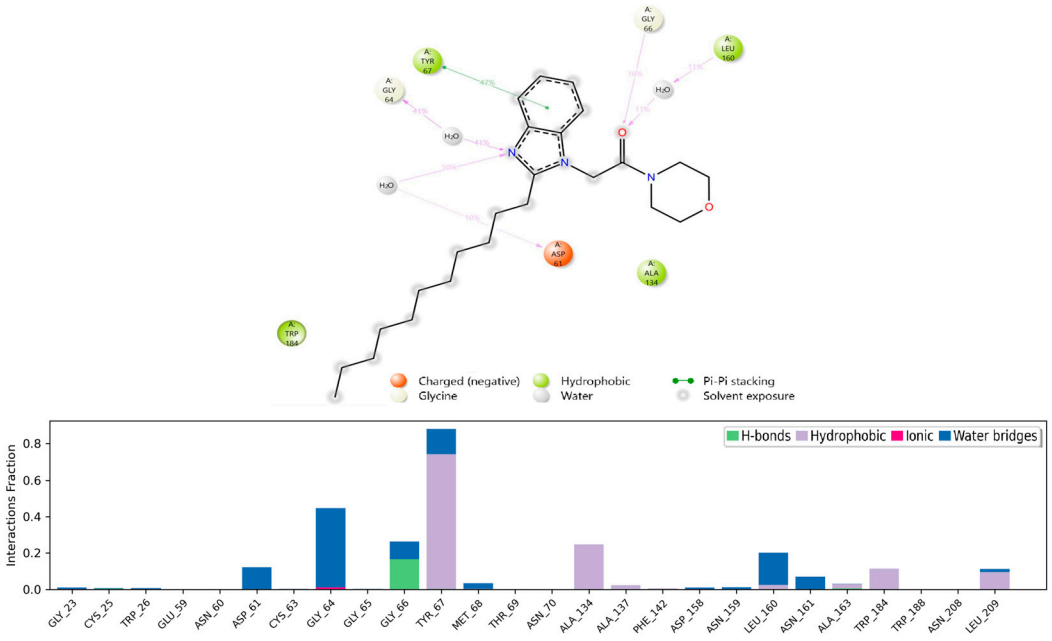


**Figure 9.** The interaction dynamics. Bonds and amino acid residues that contributed significantly (>10%) to the final conformation (top) and a list of amino acid residues and their interaction frequencies with the ligand (below).

To assess whether the flexible hydrophobic side chain of **7i** experienced rapid fluctuations during the MD calculations that would in turn reduce the stability of the ligand on the binding site, we assessed the ligand's root mean square fluctuations (RMSF) (Figure 10). The RMSF with respect to the cathepsin K backbone (ligand fit on protein), showed that the most distant portion of the alkyl side chain (atom numbers 15-21; Figure 10) experienced some fluctuations with the terminal C15 achieving the RMSF ~4.0. Generally, **7i** remained stable at the binding pocket with minimal fluctuations [59]. The orientation of the alkyl side chain was maintained by 1) the dominant TYR-67 pi-pi interaction with the benzene ring of the **7i**'s indole ring, 2) the water bridge-assisted hydrogen

 doi:10.20944/preprints202502.1264.v1



bonding between the pyrrole ring of **7i** and ASP-61/GLY-64 (Figure 9 above), and 3) the hydrophobic interaction of TRP-184 and the side chain.

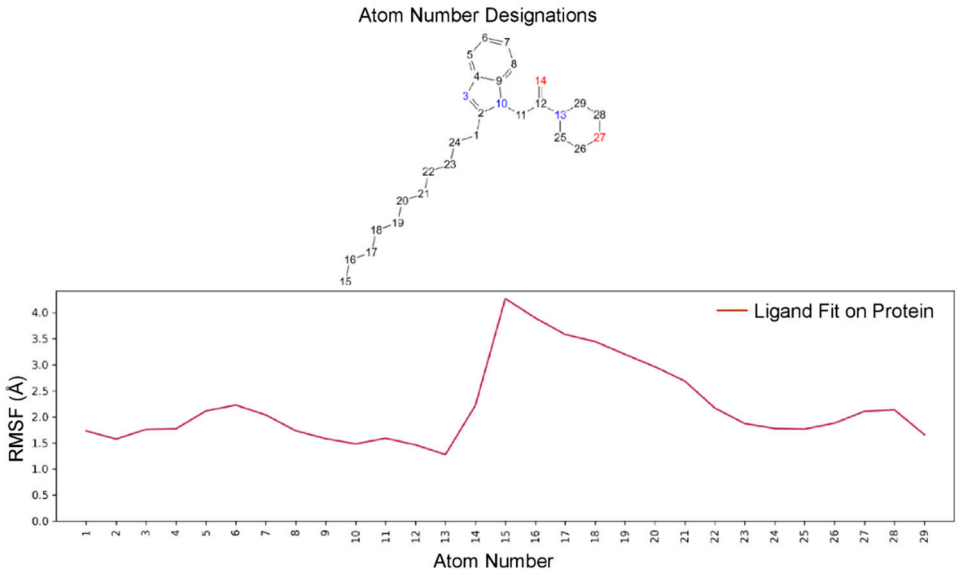


**Figure 10.** The comprehensive analysis of the stability of individual atoms of **7i** during the MD simulation.

## 3. Materials and Methods

### *3.1. Chemical Synthesis*

#### 3.1.1. General Procedures

All chemicals and solvents were purchased from Sigma-Aldrich and used without further purification. The boiling range of the petroleum ether used was 40-60 °C. Thin layer chromatography (TLC): silica gel 60 F254 plastic plates (E. Merck, layer thickness 0.2 mm) detected by UV absorption. Elemental analyses were performed on a Flash EA-1112 instrument. Melting points were determined on a Buchi 510 melting-point apparatus and the values are uncorrected. The mass spectra were measured with a KRATOS Analytical Kompact. MALDI 1: spectrometer using 2,5 di-hydroxy benzoic acid (DHB) as matrix. $^{1}$H and $^{13}$C NMR spectra were recorded at 400 MHz and 100 MHz, respectively (Bruker AC 400) in $CDCl_3$ and DMSO solution with tetramethylsilane as an internal standard. 2-Undecyl-1*H*-benzimidazole (**1**), methyl 2-(2-undecyl-1*H*-benzimidazol-1-yl) acetate (**4**) and 2-(2-undecyl-1*H*-benzimidazol-1-yl)ethanhydrazide (**5**) were prepared according to reported literature [54,61].

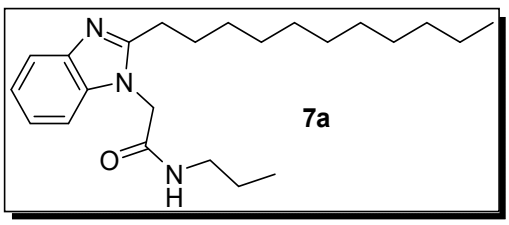


#### 3.1.2. ***N*-Propyl-2-(2-undecyl-1*H*-benzimidazol-1-yl)acetamide (7a)**

Colorless crystals, yield 62 %. mp 89-90 °C. $^{1}$H NMR spectrum, (400 MHz, $CDCl_3$), δ, ppm (*J*, Hz): 0.72-0.85 (m, 6 H, 2 $CH_3$), 1.13-1.21 (m, 16 H, 8 $CH_2$), 1.34-1.47 (m, 2 H, $CH_2$), 2.06-2.74 (m, 2 H, $CH_2$), 3.04-3.14 (m, 2 H, $NCH_2$), 4.71 (s, 2 H, $NCH_2$), 6.18 (bs, 1 H, NH), 7.15-7.61 (m, 4 H, Ar-H). $^{13}$C-NMR (100.0 MHz, $CDCl_3$), δ, ppm: 11.4, 14.1 (2 $CH_3$), 22.7, 22.8, 22.9, 23.1, 25.9, 29.3, 29.6, 29.7, 29.9, 31.8, 31.9 (11 $CH_2$), 36.8, 41.4 (2 $NCH_2$), 109.3, 118.7, 122.9, 123.1, 134.2, 141.2, 155.5 (Ar-C), 166.4 (CO).

 doi:10.20944/preprints202502.1264.v1



MS (MALDI, positive mode, matrix DHB) m/z: (M + Found: Na)+ 394.2. Anal. Calcd. For $C_{23}H_{37}N_3O$ (371.57) C, 74.35; H, 10.04; N, 11.31. C, 74.62; H, 10.40; N, 10.98.

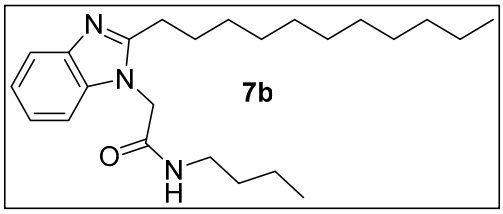


3.1.3. ***N*-Butyl-2-(2-undecyl-1*H*-benzimidazol-1-yl)acetamide** (**7b**).

Colorless crystals, yield 56 %. 83-84 °C. $^1$H NMR spectrum, (400 MHz, $CDCl_3$), δ, ppm (J, Hz): 0.81-0.88 (m, 6 H, 2 $CH_3$), 1.15-1.28 (m, 20 H, 10 $CH_2$), 1.35-1.42 (m, 4 H, 2 $CH_2$), 3.08-3.18 (m, 2 H, $NCH_2$), 4.75 (s, 2 H, $NCH_2$), 6.41 (bs, 1 H, NH), 7.15-7.27 (m, 4 H, Ar-H). $^{13}$C-NMR (100.0 MHz, $CDCl_3$), δ, ppm: 13.7 ($CH_3$), 14.1 ($CH_3$), 20.0, 22.6, 23.1, 29.3, 29.4, 29.6, 31.5 (13 $CH_2$), 39.3, 39.4 (2 $NCH_2$), 109.4, 118.5, 122.9, 123.1, 134.6, 140.9, 155.5 (Ar-C), 166.3 (CO). MS (MALDI, positive mode, matrix DHB) m/z: (M + Na)+ 408.3 Anal. Calcd. For $C_{24}H_{39}N_3O$ (385.59) C, 74.76; H, 10.20; N, 10.90. Found: C, 74.80; H, 9.87; N, 11.06.

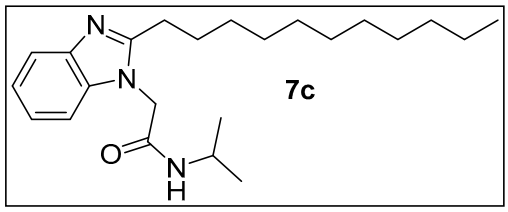


3.1.4. ***N*-Isopropyl-2-(2-undecyl-1*H*-benzimidazol-1-yl)acetamide** (**7c**).

Colorless crystals, yield 71 %. mp 92-93 °C. $^1$H NMR spectrum, (400 MHz, CDCl3), δ, ppm (*J*, Hz): 0.76-0.80 (m, 3 H, $CH_3$), 0.97 (d, *J*= 8.4, 3 H, $CH_3$), 1.05 (d, *J*= 8.8, 3 H, $CH_3$), 1.15-1.19 (m, 16 H, 8 $CH_2$), 1.49-1.54 (m, 1 H, $CH_2$), 1.70-1.75 (m, 1 H, $CH_2$), 2.01-2.06 (m, 1 H, $CH_2$), 2.70-2.75 (m, 1 H, $CH_2$), 3.92-4.04 (m, 1 H, NCH), 4.67 (s, 2 H, $NCH_2$), 5.98 (bs, 1 H, NH), 7.15-7.19 (m, 3 H, Ar-H), 7.61-7.64 (m, 1 H, Ar-H). $^{13}$C-NMR (100.0 MHz, $CDCl_3$), δ, ppm: 14.1 ($CH_3$), 22.4, 22.6 (2 $CH_3$), 22.7, 22.8, 25.8, 27.6, 29.2, 29.3, 29.4, 29.5, 29.6, 31.9 (10 $CH_2$), 37.0 (NCH), 41.9 ($NCH_2$), 109.3, 118.9, 123.1, 123.3, 134.5, 141.2, 155.4 (Ar-C), 165.4 (CO). MS (MALDI, positive mode, matrix DHB) m/z: (M + Na)+ 394.5. Anal. Calcd. For $C_{23}H_{37}N_3O$ (371.57) C, 74.35; H, 10.04; N, 11.31; Found: C, 74.62; H, 9.99; N, 11.52.

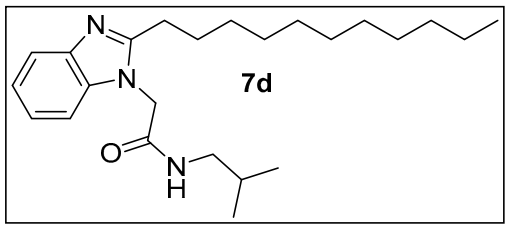


3.1.5. ***N*-Isobutyl-2-(2-undecyl-1*H*-benzimidazol-1-yl)acetamide** (**7d**).

Colorless crystals, yield 66 %.mp 87-88 °C. 1H NMR spectrum, (400 MHz, CDCl3), δ, ppm (J, Hz): 0.69-0.71 (d, 6 H, *J*= 8.8, 2$CH_3$), 0.77-0.80 (m, 3 H, $CH_3$), 0.77-0.80 (m, 3 H, $CH_3$), 1.15-1.23 (m, 16 H, 8 $CH_2$), 1.50-1.58 (m, 1 H, CH), 1.60-1.69 (m, 1 H, CH), 1.70-1.76 (m, 1 H, CH), 2.06-2.11 (m, 1 H, CH), 2.71-2.99 (m, 5 H, NCH, 2 $CH_2$), 4.73 (s, 2 H, $NCH_2$), 5.97 (bs, 1 H, NH), 7.16-7.22 (m, 3 H, Ar-H), 7.59-7.63 (m, 1 H, Ar-H). $^{13}$C-NMR (100.0 MHz, CDCl3), δ, ppm: 14.1 ($CH_3$), 20.1 (2 $CH_3$), 22.7, 23.2, 25.9, 28.3, 28.4 (5 $CH_2$), 28.5 (CH), 29.0, 29.3, 29.4, 29.5, 31.9 (5 $CH_2$), 36.9 ($NCH_2$), 47.0 (NCH), 109.7, 118.1, 123.4, 123.5, 134.2, 155.3 (Ar-C), 166.1 (CO). MS (MALDI, positive mode, matrix DHB) m/z: (M + Na)+ 408.5 Anal. Calcd. For $C_{24}H_{39}N_3O$ (385.59) C, 74.76; H, 10.20; N, 10.90; Found: C, 75.03; H, 10.09; N, 11.14.

 doi:10.20944/preprints202502.1264.v1



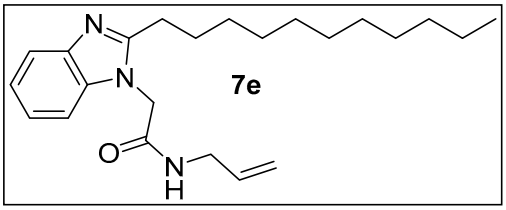


3.1.6. ***N*-Allyl-2-(2-undecyl-1*H*-benzimidazol-1-yl)acetamide (7e).**

Colorless crystals, yield 59 %. mp 78-80 °C. $^{1}$H NMR spectrum, (400 MHz, $CDCl_3$), δ, ppm (*J*, Hz): 0.77-0.82 (m, 3 H, $CH_3$), 1.17-1.19 (m, 16 H, 8 $CH_2$), 1.51-1.54 (m, 1 H, CH), 1.71-1.74 (m, 1 H, CH), 2.09-2.14 (m, 1 H, CH), 2.67-2.72 (m, 1 H, CH), 3.75-3.78 (m, 2 H, $NCH_2$), 4.73 (s, 2 H, $NCH_2$), 4.96-5.12 (m, 2 H, $CH_2$), 5.66-5.80 (m, 1 H, CH), 6.47 (bs, 1 H, NH), 7.11-7.23 (m, 3 H, Ar-H), 7.57-7.60 (m, 1 H, Ar-H). $^{13}$C-NMR (100.0 MHz, $CDCl_3$), δ, ppm: 14.1 ($CH_3$), 22.6, 23.0, 25.8, 29.3, 29.6, 31.9, 36.6 (10 $CH_2$), 41.7, 42.0 (2 $NCH_2$), 109.1, 116.0, 116.1, 116.5, 142.2, 155.6 (Ar-C, $CH=CH_2$), 166.7 (CO MS (MALDI, positive mode, matrix DHB) m/z: (M + Na)+ 392.5. Anal. Calcd. For $C_{23}H_{35}N_3O$ (369.55) C, 74.75; H, 9.55; N, 11.37. Found: C, 74.80; H, 9.33; N, 10.96.

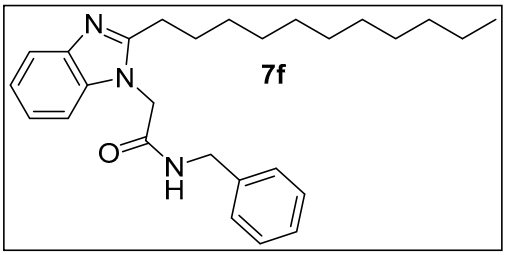


3.1.7. ***N*-Benzyl-2-(2-undecyl-1*H*-benzimidazol-1-yl)acetamide (7f).**

Colorless crystals, yield 71 %. mp 101-102 °C. $^{1}$H NMR spectrum, (400 MHz, $CDCl_3$), δ, ppm (*J*, Hz): 0.77-0.81 (m, 3 H, $CH_3$), 1.16-1.21 (m, 16 H, 8 $CH_2$), 1.14-1.54 (m, 2 H, $CH_2$), 4.25-4.31 (m, 2 H, $NCH_2$), 4.66 (s, 2 H, $NCH_2$), 6.41 (bs, 1 H, NH), 7.11-7.13 (m, 3 H, Ar-H), 7.18-7.24 (m, 5 H, Ar-H), 7.37-7.41 (m, 1 H, Ar-H). $^{13}$C-NMR (100.0 MHz, $CDCl_3$), δ, ppm: 12.5, 12.7 (2 $CH_3$), 14.2 ($CH_3$), 22.5, 22.7, 25.6, 29.3, 29.5, 29.6, 31.9, 33.1 (10 $CH_2$), 36.7, 43.5 (2 $NCH_2$), 127.3, 127.7, 128.1, 128.5, 128.8, 129.1, 130.0, 130.8, 135.7, 137.6, 138.2, 138.4, 155.5 (Ar-C), 162.3 (CO). MS (MALDI, positive mode, matrix DHB) m/z: (M + Found: Na)+ 442.5. Anal. Calcd. For $C_{27}H_{37}N_3O$ (419.61) C, 77.28; H, 8.89; N, 10.01. C, 76.95; H, 9.02; N, 10.34.

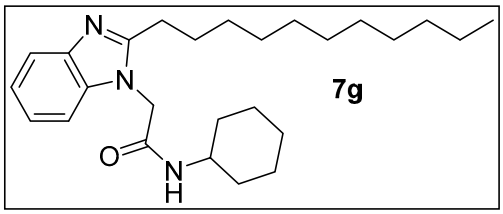


3.1.8. **N-Cyclohexyl-2-(2-undecyl-1*H*-benzimidazol-1-yl)acetamide (7g).**

Colorless crystals, yield 63 %. mp 97-98 °C. $^{1}$H NMR spectrum, (400 MHz, $CDCl_3$), δ, ppm (*J*, Hz): 0.77-0.82 (m, 3 H, $CH_3$), 0.81-1.22 (m, 20 H, 10 $CH_2$), 1.28-1.85 (m, 8 H, 4 $CH_2$), 2.05-2.08 (m, 1 H, CH), 2.71-2.77 (m, 1 H, CH), 3.62-3.72 (m, 1 H, NHCH), 4.68 (s, 2 H, $NCH_2$), 5.76 (bs, 1 H, NH), 7.17-7.19 (m, 3 H, Ar-H), 7.63-7.66 (m, 1 H, Ar-H). $^{13}$C-NMR (100.0 MHz, $CDCl_3$), δ, ppm: 14.1 ($CH_3$), 22.7, 24.9, 25.4, 25.5, 25.9, 29.3, 29.6, 31.9, 33.1, 33.2 (10 $CH_2$), 37.0 ($NCH_2$), 48.3 (NCH), 109.2, 119.0, 122.9, 123.1, 131.2, 134.6, 155.5 (Ar-C), 165.4 (CO). MS (MALDI, positive mode, matrix DHB) m/z: (M + Na)+ 434.5 Anal. Calcd. For $C_{26}H_{41}N_3O$ (411.63) C, 75.86; H, 10.04; N, 10.21; Found: C, 75.53; H, 10.11; N, 10.34.

 doi:10.20944/preprints202502.1264.v1



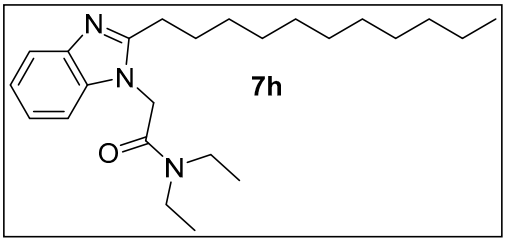


3.1.9. ***N,N*-Diethyl-2-(2-undecyl-1*H*-benzimidazol-1-yl)acetamide (7h).**

Colorless crystals, yield 57 %. mp 84-86 °C. $^{1}$H NMR spectrum, (400 MHz, $CDCl_3$), δ, ppm (*J*, Hz): 0.77-0.81 (m, 3 H, $CH_3$), 1.00-1.11 (m, 6 H, 2 $CH_3$), 1.16-1.17 (m, 16 H, 8 $CH_2$), 1.52-1.55 (m, 1 H, CH), 170-1.77 (m, 1H, CH), 2.18-2.25 (m, 1 H, CH), 2.67-2.76 (m, 1 H, CH), 3.18-3.36 (m, 4 H, 2 $NCH_2$), 4.76 (s, 2 H, $NCH_2$), 7.05-7.18 (m, 3 H, Ar-H), 7.60-7.64 (m, 1 H, Ar-H). $^{13}$C-NMR (100.0 MHz, $CDCl_3$), δ, ppm: 12.5, 12.7 (2 $CH_3$), 14.1 ($CH_3$), 22.5, 22.7, 25.6, 29.3, 29.5, 29.6, 31.9, 33.1 (10 $CH_2$), 40.1, 42.0, 42.1 (3 $NCH_2$), 117.5, 118.6, 134.6, 135.0, 135.7, 155.4 (Ar-C), 164.6 (CO). MS (MALDI, positive mode, matrix DHB) m/z: (M + Found: Na)+ 408.5. Anal. Calcd. For $C_{24}H_{39}N_3O$ (385.59) C, 74.76; H, 10.20; N, 10.90. C, 74.45; H, 10.08; N, 11.21.

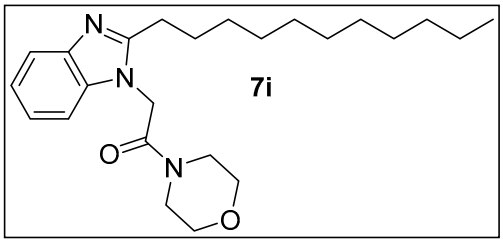


3.1.10. **1-Morpholino-2-(2-undecyl-1*H*-benzimidazol-1-yl)ethan-1-one (7i).**

Colorless crystals, yield 63 %. mp 99-101 °C. $^{1}$H NMR spectrum, (400 MHz, $CDCl_3$), δ, ppm (J, Hz): 0.78-0.82 (m, 3 H, $CH_3$), 1.16-1.21 (m, 16 H, 8 $CH_2$), 1.49-1.56 (m, 1 H, $CH_2$), 1.72-1.80 (m, 1 H, $CH_2$), 2.22 (t, *J*= 8.0 Hz, 1 H, $CH_2$), 2.64-4.72 (m, 1 H, $CH_2$), 3.53-3.67 (m, 8 H, 4 $CH_2$ morph.), 4.78 (s, 2 H, $NCH_2$), 7.02-7.19 (m, 3 H, Ar-H), 7.61-7.66 (m, 1 H, Ar-H). $^{13}$C-NMR (100.0 MHz, $CDCl_3$), δ, ppm: 14.1 ($CH_3$), 22.7, 25.3, 29.2, 29.3, 29.4, 29.5, 29.6, 29.7, 31.9, 33.2 (10 $CH_2$), 41.8 (2$NCH_2$), 46.0 ($NCH_2CO$), 66.7, 67.0 ($OCH_2$), 108.7, 119.0, 122.4, 122.6, 135.1, 135.5, 155.6 (Ar-C), 164.4 (CO). MS (MALDI, positive mode, matrix DHB) m/z: (M + Na)+ 422.5 Anal. Calcd. For $C_{24}H_{37}N_3O$ (399.58) C, 72.14; H, 9.33; N, 10.52; Found: C, 71.80; H, 9.53; N, 10.26.

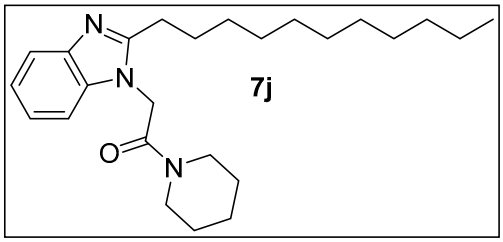


3.1.11. **1-(Piperidin-1-yl)-2-(2-undecyl-1*H*-benzimidazol-1-yl)ethan-1-one (7j).**

Colorless crystals, yield 59 %. mp 107-108 °C. $^{1}$H NMR spectrum, (400 MHz, $CDCl_3$), δ, ppm (*J*, Hz): 0.78-0.82 (m, 3 H, $CH_3$), 1.17-1.22 (m, 16 H, 8 $CH_2$), 1.45-1.50 (m, 2 H, $CH_2$), 1.53-1.60 (m, 2 H, $CH_2$), 1.63-1.73 (m, 4 H, 2 $CH_2$), 2.21-2.26 (m, 1 H, CH), 2.69-2.76 (m, 1 H, CH), 3.39-3.52 (m, 4 H, 2 $CH_2$), 4.79 (s, 2 H, $NCH_2$), 7.07-7.16 (m, 3 H, Ar-H), 7.61-7.66 (m, 1 H, Ar-H). $^{13}$C-NMR (100.0 MHz, $CDCl_3$), δ, ppm: 14.1 ($CH_3$), 20.3, 22.7, 24.1, 24.4, 24.7, 25.4, 25.5, 25.6, 26.4, 26.6, 27.4, 29.6, 31.9 (13 $CH_2$), 39.8, 44.3, 46.8 (3 $NCH_2$), 118.7, 119.0, 122.1, 122.4, 135.2, 141.8, 155.7 (Ar-C), 164.0 (CO). MS (MALDI, positive mode, matrix DHB) m/z: (M + Found: Na)+ 420.6 Anal. Calcd. For $C_{25}H_{39}N_3O$ (397.61) C, 75.52; H, 9.89; N, 10.57; C, 75.81; H, 10.11; N, 10.26.

 doi:10.20944/preprints202502.1264.v1



*3.2. Biological Experimentation*

3.2.1. Cell Culture

Four human cancer cell lines (A549, MDA-MB 231, MCF-7, U87) and HEK293 were purchased from the American Type Culture Collection (ATCC, Manassas, VA, USA). Cells were grown in Dulbecco's modified Eagle's medium (DMEM; Wako, Japan) supplemented with 100 IU/mL penicillin (Invitrogen), 100 µg/mL streptomycin (Invitrogen), non-essential amino acids (Invitrogen, USA), and 10% fetal bovine serum (FBS; Gibco). The cells were maintained at 37°C in a 5% CO2 incubator.

3.2.2. MTT Assay

The tetrazolium-based MTT assay was performed for cytotoxicity check as described with modification [62]. In brief, cells seeded in a 96-well plate were treated with serial dilutions (1000 to 1.0 µg/mL) of each compound or complete medium as a control for 24 h at 37°C. MTT reagent (Thermo Fisher Scientific, Wilmington, DE, USA) was added to the cells (0.5 mg/ml) and incubated for 4 h. The medium containing MTT reagent was removed, and the formed purple crystals of formazan were solubilized in DMSO. The number of living cells in each well was determined using a microplate reader. The absorbance was measured at 570 nm and was run in triplicates. Percent cell viability compared to the control was calculated for each dilution of the tested compounds and the cytotoxic concentration 50% (CC50) values were determined by SPSS probit analysis in SPSS software (SPSS Inc., Chicago, IL). Experimental results are expressed as mean ± SEM.

3.2.3. Ligand Lipophilic Efficiency (LLE)

LLE is an assessment tool that evaluates the balance between a compound's in vitro potency and lipophilic nature [63]. LLE was calculated using the following formula:

$$LLE = pIC50 - clogP \text{ or } D$$

The pIC50 values were determined using the following formula:

$$pIC50 = -\log10 (IC50 \text{ in } M)$$

The values of clogP were estimated via SwissADME (http://www.swissadme.ch/); "URL (accessed on 29 November 2024),", and the calculation of LLE was executed using Excel spreadsheet. A promising hit should have a positive LLE value above 3 with clogP values in the range of 2-3 [64–66].

*3.3. In-Silico Studies*

3.3.1. Docking Studies

3D Crystal Structure

The X-ray coordinates of Human cathepsin K (PDBID:1BGO, Resolution: 2.30 Å) in complex with a covalent peptidomimetic inhibitor (I10 300) was extracted from the PDB database (https://www.rcsb.org/, accessed on 07 July 2024).

3.3.2. Protein Preparation and Docking Validation

The PDB structure was prepared for docking using the Protein Preparation Workflow from Schrödinger Release 2021-3: Protein Preparation Wizard, Schrödinger, LLC, New York, NY, 2021 [60]. During the process of preparation and minimization, the pH value was adjusted to 7.4. When necessary, adjustments were made to the ionization state. Polar hydrogen atoms were added, and redundant water molecules were removed in the structures. The receptors were refined in the OPLS3 force field to prepare them for docking. The final step was the optimization and minimization of the

 doi:10.20944/preprints202502.1264.v1



ligand-protein complexes using an OPLS3 force field and an RMSD threshold of 0.30 Å for atoms that did not contain hydrogen. Receptor grid generation was determined by taking the three-dimensional coordinates of the active site of cathepsin K, at (36.85, 14.99, -9.46) for the x, y, and z dimensions, respectively, and within a constrained length of 20 Å, a centroid in the workspace in the active site of the receptor was created and a grid box was defined. Next, a receptor grid was prepared with a van der Waals radius set to 1.00. The binding site was enclosed in the grid box with a size of 20 Å each axis with no constraints. Lastly, the docking process was iterated and validated using three different parameters that were introduced while screening. Subsequently, the lowest binding energy conformation was determined while the pose was aligned to the conformation appearing in the crystallographic structure by using the structure superimposition feature of Maestro. The RMSD of the alignments were subsequently calculated, and the docking procedure was repeated and validated using three distinct screening configurations.

#### 3.3.3. Ligand Library Preparation

The 10 compounds were prepared using the LigPrep tool in Maestro to add missing hydrogen \their respective 3D chemical structures and ionize stereoisomers at a neutral pH of 7.0 ± 2.0 using Epik. Generation of tautomer and desalt were checked, and the stereoisomers were left to contain specific chirality and to produce at most 32 isomers per ligand were subsequently used for docking [59,60].

#### 3.3.4. Molecular Docking Using Induced-Fit Docking (IFD)

The Induced-fit docking tool in Maestro first docks each ligand using a softened potential, van der Waals radii scaling, and flexible conformational sampling. Side-chain prediction for a specified distance around every ligand pose is performed next [59,60]. In this process, residues and the ligand in every protein/ligand complex pose are minimized. It finally predicts a favorable binding pose based on the IFD score.

#### 3.3.5. Molecular Dynamics Calculation

The top hit compound identified by the biological and IFD assessments was subsequently presented to the molecular dynamics (MD) Desmond workflow in Maestro 13.6 software (Schrödinger Release 2023-2) [60]. Utilizing the Desmond System Builder, a simulation system generated in the TIP3P solvent model made of a buffer system comprising 0.15M sodium chloride. The receptor-ligand complex was immersed in this solvent and the system was duly minimized through the OPLS4 force field. This resulted in the final system made of about 25,000 atoms. The whole system was then retrieved and relaxed through the default protocol and heated at 310K while kept under the constant pressure of 1.103 bar. Other parameters including the Coulombic cutoff distance were kept at default settings followed by MD simulation for 100 ns. The Desmond Simulation Interaction Diagram tool was then used to load and analyze the results following the MD calculations.

## 4. Conclusions

A series of ten novel *N*-alkyl-2-(2-undecyl-1*H*-benzimidazol-1-yl) acetamides were synthesized from 2-(2-undecyl-1*H*-benzimidazol-1-yl)ethanhydrazide using the azide coupling process with a variety of amines. The novel chemicals were developed to prevent breast cancer cell proliferation by inhibiting cathepsin K. The compounds were examined for antiproliferative activity on four cancer cell lines: A549, MDA-MB231, MCF-7, U87, and HEK293 to determine their relative degree of inhibition. The results showed that most compounds had higher activity against MDA-MD231 than against other cell lines. Compounds **7h**, **7i**, **7a**, and **7j** demonstrated the strongest inhibition, with IC50s of 17, 27, 38, and 67 µg/ml, respectively. In terms of degree of inhibition, compounds **7a** and **7j** demonstrated the highest selectivity to MDA-MD231. Molecular docking supported cathepsin K-

 doi:10.20944/preprints202502.1264.v1



mediated activity, with compound **7i** having highest affinity to the target and submitted to the MD interrogation. Compound **7i** showed a well equilibrated and stable complex with cathepsin K, largely maintained by aromatic stabilization between its indole ring and TYR-67 of cathepsin K. Furthermore, lipophilicity's impact on activity was assessed using LLE calculations, which revealed that **7i** displayed optimal potency with moderate lipophilicity. Based on these findings, the developed compounds are promising antiproliferative agents for invasive breast cancer where a cathepsin inhibition pathway could be postulated.

**Supplementary Materials:** The following supporting information can be downloaded at: www.mdpi.com/xxx/s1, Figure S1 $^{1}$HNMR of 7a. Figure S2 $^{13}$C HNMR of 7a. Figure S3 MALDI MS spectra of 7a. Figure S4 $^{13}$C HNMR of 7b. Figure S5 MALDI MS spectra of 7b. Figure S6 $^{1}$HNMR of 7c. Figure S7 $^{13}$C HNMR of 7c. Figure S8 MALDI MS spectra of 7c. Figure S9 $^{1}$HNMR of 7d. Figure S10 $^{13}$C HNMR of 7d. Figure S11 MALDI MS spectra of 7d. Figure S12 $^{1}$HNMR of 7e. Figure S13 $^{13}$C HNMR of 7e. Figure S14 MALDI MS spectra of 7e. Figure S15 $^{1}$ HNMR of 7f. Figure S16 $^{13}$C HNMR of 7f. Figure S17 MALDI MS spectra of 7f.

**Author Contributions:** For research articles with several authors, a short paragraph specifying their individual contributions must be provided. The following statements should be used "Conceptualization, A.H.A.K., S.R., M.G., M.S. and I.A.; methodology, A.H.A.K., I.A., W.F., M.S., A.M., A.A., M.S. and M.G..; software, M.A., T.R., and M.G.; validation, W.F., N.T., A.M. and A.Z.; formal analysis, A.H.A.K., M.S., A.M. and M.S.; investigation, A.H.A.K., I.A., N.T., M.S. and M.T.; resources, S.R., M.A., A.M. and T.R.; data curation, A.H.A.K., S.R., N.T. A.A., and M.A.; writing—original draft preparation, A.H.A.K., M.K., S.A., M.G., M.A., A.M., M.S., N.T., F.A., M.Z., T.R. and W.F.; writing—review and editing, M.K., S.A., M.G., M.A., A.M., M.S., N.T., F.A., M.Z., T.R. and W.F; visualization, A.H.A.K.; supervision, A.H.A.K., M.A., S.R., A.M. and M.G..; project administration, A.H.A.K., N.T., and A.A..; funding acquisition, A.H.A.K., M.A., I.A., T.R. and A.M. All authors have read and agreed to the published version of the manuscript." Please turn to the CRediT taxonomy for the term explanation. Authorship must be limited to those who have contributed substantially to the work reported.

**Funding:** This research received no external funding

**Informed Consent Statement:** Not applicable.

**Data Availability Statement:** In silico drug experiments using molecular docking to target Human cathepsin K (PDBID:1BGO, Resolution: 2.30 Å) in complex with a covalent peptidomimetic inhibitor (I10 300) was obtained from the Research Collaboratory for Structural Bioinformatics (RCSB) Protein Data Bank (PDB). PDB DOI: https://doi.org/10.2210/pdb1BGO/pdb. All data generated or analyzed during this study are included in this published article.

**Conflicts of Interest:** The authors declare no conflicts of interest.

## References

1. Deepak, K.G., Vempati, R.; Nagaraju, G.P.; Dasari, V.R.; Nagini, S.; Rao, D.N.; Malla, R.R. Tumor microenvironment: Challenges and opportunities in targeting metastasis of triple negative breast cancer. *Pharmacological research* **2020**,153,104683. https://doi.org/10.1016/j.phrs.2020.104683.
2. Sloane, B.F.; List, K.; Fingleton, B.; Matrisian, L. Proteases in Cancer: Significance for Invasion and Metastasis. *Proteases: Structure and Function* **2013**, 491-550. https://doi.org/10.1007/978-3-7091-0885-7_15.
3. Gondi C.S.;, Rao, J.S. Cathepsin B as a cancer target. *Expert opinion on therapeutic targets* **2013**, 17(3),281-91. https://doi.org/10.1517/14728222.2013.740461.
4. Seo, S.U.; Woo, S.M.; Im, S.S.; Jang, Y.; Han, E.; Kim, S.H.; Lee, H.; Lee, H.S.; Nam, J.O.; Gabrielson, E.; Min, K.J. Cathepsin D as a potential therapeutic target to enhance anticancer drug-induced apoptosis via RNF183-mediated destabilization of Bcl-xL in cancer cells. *Cell Death & Disease*. **2022,** *13*(2), 115. https://doi.org/10.1038/s41419-022-04581-7.
5. Lee, S.G.; Woo, S.M.; Seo, S.U.; Lee, C-H.; Baek, M-C.; Jang, S.H.; Park, Z.Y.; Yook, S.; Nam, J-O.; Kwon, T.K. Cathepsin D promotes polarization of tumor-associated macrophages and metastasis through TGFBI-

CCL20 signaling. *Experimental & Molecular Medicine*. **2024**, *56*(2), 383-394. https://doi.org/10.1038/s12276-024-01163-9.

6. Lecaille, F.; Chazeirat, T.; Saidi, A.; Lalmanach, G. Cathepsin V: Molecular characteristics and significance in health and disease. *Molecular Aspects of Medicine*. **2022**, *88*, 101086. https://doi.org/10.1016/j.mam.2022.101086.
7. Gall, C.L.; Bellahcene, A.; Bonnelye, E.; Gasser, J.A.; Castronovo, V.; Green, J.; Zimmermann, J.; Clezardin, P. A cathepsin K inhibitor reduces breast cancer–induced osteolysis and skeletal tumor burden. *Cancer research* **2007**, *67*(20), 9894-9902. https://doi.org/10.1158/0008-5472.CAN-06-3940.
8. Dai, R.; Wu, Z.; Chu, H.Y.; Lu, J.; Lyu, A.; Liu, J.; Zhang, G. Cathepsin K: the action in and beyond bone. *Frontiers in cell and developmental biology* **2020**, *8*, 433. https://doi.org/10.3389/fcell.2020.00433.
9. Duong, L.T.; Wesolowski, G.A.; Leung, P.; Oballa, R.; Pickarski, M. Efficacy of a cathepsin K inhibitor in a preclinical model for prevention and treatment of breast cancer bone metastasis. *Molecular cancer therapeutics* **2014**, *13*(12), 2898-2909. https://doi.org/10.1158/1535-7163.MCT-14-0253.
10. Chen, B.; Platt, M.O. Multiplex zymography captures stage-specific activity profiles of cathepsins K, L, and S in human breast, lung, and cervical cancer. *Journal of translational medicine* **2011**, *9*, 1-13. https://doi.org/10.1186/1479-5876-9-109.
11. Andrade, S.S.; Gouvea, I.E.; Silva, M.C.C.; Castro, E.D.; de Paula, C.A.A.; Okamoto, D.; Oliveira, L.; Peres, G.B.; Ottaiano, T.; Facina, G.; Nazario, A.C.P.; Campos, A.H. J.F.M.; Paredes-Gamer, E.J.; Juliano, M.; da Silva, I.D.C.G.; Oliva, M.L.V.; Girao, M.J.B C. Cathepsin K induces platelet dysfunction and affects cell signaling in breast cancer-molecularly distinct behavior of cathepsin K in breast cancer. *BMC cancer* **2016**, *16*, 1-19. https://doi.org/10.1186/s12885-016-2203-7.
12. Teitelbaum, S.L. Bone resorption by osteoclasts. *Science* **2000**, *289*(5484), 1504-1508. DOI: 10.1126/science.289.5484.1504.
13. Takatani-Nakase, T.; Matsui, C.; Hosotani, M.; Omura, M.; Takahashi, K.; Nakase, I. Hypoxia enhances motility and EMT through the Na+/H+ exchanger NHE-1 in MDA-MB-231 breast cancer cells. *Experimental cell research*. **2022**, *412*(1), 113006. https://doi.org/10.1016/j.yexcr.2021.113006.
14. Saxena, K.; Jolly, M.K.; Balamurugan, K. Hypoxia, partial EMT and collective migration: Emerging culprits in metastasis. *Translational oncology*. **2020**, *13*(11), 100845. https://doi.org/10.1016/j.tranon.2020.100845.
15. Patrakova, E.; Biryukov, M.; Troitskaya, O.; Gugin, P.; Milakhina, E.; Semenov, D.; Poletaeva, J.; Ryabchikova, E.; Novak, D.; Kryachkova, N.; Polyakova, A.; Zhilnikova, M.; Zakrevsky, D.; Schweigert, I.; Koval, O. Chloroquine enhances death in lung adenocarcinoma A549 cells exposed to cold atmospheric plasma jet. *Cells*. **2023**, *12*(2), 290. https://doi.org/10.3390/cells12020290.
16. Seker-Polat, F.; Degirmenci, N.P.; Solaroglu, I.; Bagci-Onder, T. Tumor cell infiltration into the brain in glioblastoma: from mechanisms to clinical perspectives. *Cancers*. **2022**, *14*(2), 443. https://doi.org/10.3390/cancers14020443.
17. Wang, J.; Zheng, M.; Yang, X.; Zhou, X.; Zhang, S. The role of Cathepsin B in pathophysiologies of non-tumor and tumor tissues: a systematic review. *Journal of Cancer*. **2023**, *14*(12), 2344–2358. https://doi.org/10.7150/jca.86531.
18. Zamyatnin, A.A.; Gregory, L.C.; Townsend, P.A.; Soond, S.M. Beyond basic research: the contribution of cathepsin B to cancer development, diagnosis, and therapy. *Expert Opinion on Therapeutic Targets*. **2022**, *26*(11), 963–977. https://doi.org/10.1080/14728222.2022.2161888.
19. Qattan, M.Y.; Khan, M.I.; Alharbi, S.H.; Verma, A.K.; Al-Saeed, F.A.; Abduallah, A.M.; Al Areefy, A.A. Therapeutic importance of kaempferol in the treatment of cancer through the modulation of cell signalling pathways. *Molecules*. **2022**, *27*(24), 8864. https://doi.org/10.3390/molecules27248864.
20. Soltanian S, Riahirad H, Pabarja A, Karimzadeh MR, Saeidi K. Kaempferol and docetaxel diminish side population and down-regulate some cancer stem cell markers in breast cancer cell line MCF-7. *Biocell* **2017**, *41*(2&3),33. doi:10.32604/biocell.2017.00033.
21. Sharma, R.; Bali, A.; Chaudhari, B.B. Synthesis of methanesulphonamido-benzimidazole derivatives as gastro-sparing anti-inflammatory agents with antioxidant effect. *Bioorganic & Medicinal Chemistry Letters*. **2017**, *27*(13), 3007-3013. https://doi.org/10.1016/j.bmcl.2017.05.017.

22. Veerasamy, R.; Roy, A.; Karunakaran, R.; Rajak, H. Structure-Activity Relationship Analysis of Benzimidazoles as Emerging Anti-Inflammatory Agents: An Overview. *Pharmaceuticals.* **2021**, *14*(7), 663. https://doi.org/10.3390/ph14070663.
23. Alanazi, A.H.G.; Alam, T.; Imran, M. Design, molecular docking studies, in silico drug likeliness prediction and synthesis of some benzimidazole derivatives as antihypertensive agents. *Indo American Journal of Pharmaceutical Science.* **2017**, *4*(4), 926-936.
24. Rashid, M.; Husain, A.; Shaharyar, M.; Sarafroz, M. Anticancer activity of new compounds using benzimidazole as a scaffold. *Anti-Cancer Agents in Medicinal Chemistry (Formerly Current Medicinal Chemistry-Anti-Cancer Agents)***2014**, *14*(7), 1003-1018. PMID: 24827531 DOI:10.2174/1871520614666140509153021.
25. Wang, Z.; Deng, X.; Xiong, S.; Xiong, R.; Liu, J.; Zou, L.; Lei, X.; Cao, X.; Xie, Z.; Chen, Y.; Liu, Y.; Zheng, X.; Tang, G. Design, synthesis, and biological evaluation of chrysin benzimidazole derivatives as potential anticancer agents. *Natural product research*. **2018**, *32*(24), 2900-2909. https://doi.org/10.1080/14786419.2017.1389940.
26. Morais, G.R.; Palma, E.; Marques, F.; Gano, L.; Oliveira, M.C.; Abrunhosa, A.; Miranda, H.V.; Outeiro, T.F.; Santos, I.; Paulo, A. Synthesis and Biological Evaluation of Novel 2-Aryl Benzimidazoles as Chemotherapeutic Agents. *Journal of Heterocyclic Chemistry*. **2017**, *54*(1), 255-267. https://doi.org/10.1002/jhet.2575.
27. Shaker, Y.M.; Omar, M.A.; Mahmoud, K.; Elhallouty, S.M.; El-Senousy, W.M.; Ali, M.M.; Mahmoud, A.E.; Abdel-Halim, A.H.; Soliman, S.M.; El Diwani, H.I. Synthesis, in vitro and in vivo antitumor and antiviral activity of novel 1-substituted benzimidazole derivatives. *Journal of enzyme inhibition and medicinal chemistry*. **2015**, *30*(5), 826-845. https://doi.org/10.3109/14756366.2014.979344.
28. Archie, S.R.; Das, B.K.; Hossain, M.S.; Kumar, U.; Rouf, A.S. Synthesis and antioxidant activity of 2-substituted-5-nitro benzimidazole derivatives. *Int. J. Pharm. Pharm. Sci*. **2017**, *9*, 308-310. http://dx.doi.org/10.22159/ijpps.2017v9i1.14972.
29. Alam, F.; Dey, B.K.; Sharma, K.; Chakraborty, A.; Kalita, P. Synthesis, antimicrobial and anthelmintic activity of some novel benzimidazole derivatives. *Int. J. Drug Res. Tech.* **2014**, *4*(3), 31-38.
30. Prasad, M.C.; Kumar, S.A.; Kumar, D.S.; Kumar, S.R.; Chandra, S.S.; Kumar, G.D. Designing and Synthesis of some Novel 2-Substituted Benzimidazole Derivatives and their Evaluation for Antimicrobial and Anthelmintic Activity. *Asian Journal of Research in Chemistry*, **2019**, *12*(2), 58-62. DOI: 10.5958/0974-4150.2019.00013.0.
31. Navarrete-Vázquez, G.; Moreno-Diaz, H.; Aguirre-Crespo, F.; Leon-Rivera, I.; Villalobos-Molina, R.; Munoz-Muniz, O.; Estrada-Soto, S. Design, microwave-assisted synthesis, and spasmolytic activity of 2-(alkyloxyaryl)-1H-benzimidazole derivatives as constrained stilbene bioisosteres. *Bioorganic & Medicinal Chemistry Letters*, 2006, *16*(16), 4169-4173. https://doi.org/10.1016/j.bmcl.2006.05.082.
32. El-Gohary, N.S.; Shaaban, M.I. Synthesis and biological evaluation of a new series of benzimidazole derivatives as antimicrobial, antiquorum-sensing and antitumor agents. *European journal of medicinal chemistry* **2017**, *131*, 255-262. https://doi.org/10.1016/j.ejmech.2017.03.018.
33. Singh, L.R.; Avula, S.R.; Raj, S.; Srivastava, A.; Palnati, G.R.; Tripathi, C.K.M.; Pasupuleti, M.; Sashidhara, K.V. Coumarin–benzimidazole hybrids as a potent antimicrobial agent: synthesis and biological elevation. *The Journal of antibiotics* **2017**, *70*(9), 954-961. https://doi.org/10.1038/ja.2017.70.
34. Bansal, Y.; Kaur, M.; Bansal, G. Antimicrobial potential of benzimidazole derived molecules. *Mini Reviews in Medicinal Chemistry* **2019**, *19*(8), 624-646. DOI: https://doi.org/10.2174/1389557517666171101104024.
35. Chintakunta, R.; Meka, G. Synthesis, in silico studies and antibacterial activity of some novel 2-substituted benzimidazole derivatives. *Futur J Pharm Sci* **2020**, *6*, 128, 1-6. https://doi.org/10.1186/s43094-020-00144-9.
36. Kara, M.; Oztas, E.; Ramazanogulları, R.; Kouretas, D.; Nepka, C.; Tsatsakis, A.M.; Veskoukis, A.S. Benomyl, a benzimidazole fungicide, induces oxidative stress and apoptosis in neural cells. *Toxicology reports* **2020**, *7*, 501-509. https://doi.org/10.1016/j.toxrep.2020.04.001.
37. Dreikorn, B.A.; Owen, W.J. Fungicides, Agricultural. *Kirk-Othmer Encyclopedia of Chemical Technology* 2000. https://doi.org/10.1002/0471238961.0621140704180509.a01.

38. Liang, X.L.; Ouyang, L.; Yu, N.N.; Sun, Z.H.; Gui, Z.K.; Niu, Y.L.; He, Q.Y.; Zhang, J.; Wang, Y. Histone deacetylase inhibitor pracinostat suppresses colorectal cancer by inducing CDK5-Drp1 signaling-mediated peripheral mitofission. *Journal of pharmaceutical analysis* **2023**, *13*(10), 1168-1182. https://doi.org/10.1016/j.jpha.2023.06.005.
39. Sedky, N.K.; Hamdan, A.A.; Emad, S.; Allam, A.L.; Ali, M.; Tolba, M.F. Insights into the therapeutic potential of histone deacetylase inhibitor/immunotherapy combination regimens in solid tumors. *Clinical and Translational Oncology* **2022**, *24*(7), 1262-1273. https://doi.org/10.1007/s12094-022-02779-x.
40. Weide, R.; Hess, G.; Koppler, H.; Heymanns, J.; Thomalla, J.; Aldaoud, A.; Losem, C.; Schmitz, S.; Haak, U.; Huber, C.; Unterhalt, M.; Hiddemann, W.; Dreyling, M. High anti-lymphoma activity of bendamustine/mitoxantrone/rituximab in rituximab pretreated relapsed or refractory indolent lymphomas and mantle cell lymphomas. A multicenter phase II study of the German Low Grade Lymphoma Study Group (GLSG). *Leukemia & lymphoma* **2007**, *48*(7), 1299-1306. https://doi.org/10.1080/10428190701361828.
41. World Health Organization model list of essential medicines: 22nd list. Geneva: World Health Organization, **2021**. hdl: 10665/345533. WHO/MHP/HPS/EML.
42. Testa, B.; Crivori, P.; Reist, M.; Carrupt, P.A. The influence of lipophilicity on the pharmacokinetic behavior of drugs: Concepts and examples. *Perspectives in Drug Discovery and Design* **2000**, *19*, 179-211. https://doi.org/10.1023/A:1008741731244.
43. Morak-Młodawska, B.; Jelen, M.; Martula, E.; Korlacki, R. Study of Lipophilicity and ADME Properties of 1,9-Diazaphenothiazines with Anticancer Action. *International journal of molecular sciences* **2023**, *24*(8), 6970. Doi: 10.3390/ijms24086970.
44. Fathalla, W. Synthesis of methyl 2-[2-(4-phenyl [1, 2, 4] triazolo-[4, 3-a] quinoxalin-1-ylsulfanyl) acetamido] alkanoates and their N-regioisomeric analogs. *Chemistry of Heterocyclic Compounds* **2015**, *51*, 73-79. https://doi.org/10.1007/s10593-015-1662-0.
45. Ismail, E.F.; Ali, I.A.I.; Fathalla, W.; Alsheikh, A.A.; El Tamneya, E.S. Synthesis of methyl [3-alkyl-2-(2, 4-dioxo-3, 4-dihydro-2H-quinazolin-1-yl)-acetamido] alkanoate. *ARKIVOC: Online Journal of Organic Chemistry*, **2017**, 104-120. **DOI:** 10.3998/ark.5550190.0018.400.
46. Walid, F.; Pavel, P. Synthesis of methyl 2-[(1, 2-dihydro-4-hydroxy-2-oxo-1-phenylquinolin-3-yl) carbonylamino] alkanoates and methyl 2-[2-((1, 2-dihydro-4-hydroxy-2-oxo-1-phenylquinolin-3-yl) carbonyl-amino) alkanamido] alkanoate. *ARKIVOC: Online Journal of Organic Chemistry*, **2017**, *2017*, 158-173. DOI: http://dx.doi.org/10.3998/ark.5550190.p009.946.
47. Fathalla, W.; Pazdera, P. Convenient Synthesis of Piperazine Substituted Quinolones. *J. Heterocyclic Chem* **2017**, *54*(6), 3481-3489. https://doi.org/10.1002/jhet.2971.
48. El Rayes, S.M.; Aboelmagd, A.; Gomaa, M.S.; Ali, I.A.; Fathalla, W.; Pottoo, F.H.; Khan, F.A. Convenient Synthesis and Anticancer Activity of Methyl 2-[3-(3-Phenyl-quinoxalin-2-ylsulfanyl) propanamido] alkanoates and N-Alkyl 3-((3-Phenyl-quinoxalin-2-yl) sulfanyl) propanamides. *ACS omega* **2019**, *4*(20), 18555-18566. DOI: 10.1021/acsomega.9b02320.
49. Aboelmagd, A.; Alotaibi, S.H.; El Rayes, S.M.; Elsayed, G.M.; Ali, I.A.; Fathalla, W.; Pottoo, F.H.; Khan, F.A. Synthesis and Anti proliferative Activity of New N-Pentylquinoxaline carboxamides and Their *O*-Regioisomer. *Chemistry Select* **2020**, *5*(43), 13439-13453. https://doi.org/10.1002/slct.202003024.
50. Aboelmagd, A.; El Rayes, S.M.; Gomaa, M.S.; Ali, I.A.; Fathalla, W.; Pottoo, F.H.; Khan, F.A.; Khalifa, M.E. The synthesis and antiproliferative activity of new N-allyl quinoxalinecarboxamides and their O-regioisomers. *New Journal of Chemistry* **2021**, *45*(2), 831-849. DOI https://doi.org/10.1039/D0NJ03672B.
51. Irby, D.; Du, C.; Li, F. Lipid–drug conjugate for enhancing drug delivery. *Molecular pharmaceutics* **2017**, *14*(5), 1325-1338. https://doi.org/10.1021/acs.molpharmaceut.6b01027.
52. Han, S.; Mei, L.; Quach, T.; Porter, C.; Trevaskis, N. Lipophilic conjugates of drugs: a tool to improve drug pharmacokinetic and therapeutic profiles. *Pharmaceutical Research* **2021**, *38*(9),1497-1518.
53. Bhat, M.; Jatyan, R.; Mittal, A.; Mahato, R.I.; Chitkara, D. Opportunities and challenges of fatty acid conjugated therapeutics. *Chemistry and Physics of Lipids* **2021**, *236*, 105053. https://doi.org/10.1016/j.chemphyslip.2021.105053.

54. Hong Yao, Hong-Ping Wu, Jing Chang, Qi Lin, Tai-Bao Wei and You-Ming Zhang. A carboxylic acid functionalized benzimidazole-based supramolecular gel with multi-stimuli responsive properties. ***New J. Chem.***, **2016**, ***40***, 4940-4944 https://doi.org/10.1039/C5NJ03422A
55. Pettersson, M.; Hou, X.; Kuhn, M.; Wager, T. T.; Kauffman, G. W.; Verhoest, P. R. Quantitative assessment of the impact of fluorine substitution on P-Glycoprotein (P-GP) mediated efflux, permeability, lipophilicity, and metabolic stability. *Journal of Medicinal Chemistry* **2016**, *59*(11), 5284–5296. https://doi.org/10.1021/acs.jmedchem.6b00027.
56. Meanwell, N. A. Improving Drug Design: An Update on Recent Applications of Efficiency Metrics, Strategies for Replacing Problematic Elements, and Compounds in Nontraditional Drug Space. Chemical Research in *Toxicology* **2016**, *29*(4), 564–616. https://doi.org/10.1021/acs.chemrestox.6b00043.
57. Ferreira, L.L.G.; Andricopulo, A.D. ADMET modeling approaches in drug discovery. *Drug discovery today* **2019**, *24*(5), 1157-1165. https://doi.org/10.1016/j.drudis.2019.03.015.
58. Shelley, J.C.; Cholleti, A.; Frye, L.L.; Greenwood, J.R.; Timlin, M.R.; Uchimaya, M. Epik: a software program for $pK_a$ prediction and protonation state generation for drug-like molecules. *Journal of computer-aided molecular design* **2007**, *21*, 681-691. https://doi.org/10.1007/s10822-007-9133-z.
59. Gomaa, M.; Gad, W.; Hussein, D.; Pottoo, F.H.; Tawfeeq, N.; Alturki, M.; Alfahad, D.; Alanazi, R.; Salama, I.; Aziz, M.; et al. Sulfadiazine Exerts Potential Anticancer Effect in HepG2 and MCF7 Cells by Inhibiting TNF$\alpha$, IL1b, COX-1, COX-2, 5-LOX Gene Expression: Evidence from In Vitro and Computational Studies. *Pharmaceuticals* **2024**, *17*, 189. https://doi.org/10.3390/ph17020189.
60. Al Khzem, A.H.; Shoaib, T.H.; Mukhtar, R.M.; Alturki, M.S.; Gomaa, M.S.; Hussein, D.; Tawfeeq, N.; Bano, M.; Sarafroz, M.; Alzahrani, R.; et al. Repurposing FDA-Approved Agents to Develop a Prototype *Helicobacter pylori* Shikimate Kinase (HPSK) Inhibitor: A Computational Approach Using Virtual Screening, MM-GBSA Calculations, MD Simulations, and DFT Analysis. *Pharmaceuticals* **2025**, *18*, 174. https://doi.org/10.3390/ph18020174
61. Hong Yao, Jiao Wang, Shan-Shan Song, Yan-Qing Fan, Xiao-Wen Guan, Qi Zhou, Tai-Bao Wei, Qi Lin and You-Ming Zhang. A novel supramolecular AIE gel acts as a multi-analyte sensor array. ***New J. Chem.***, **2018**, ***42***, 18059-18065. https://doi.org/10.1039/C8NJ04160A
62. Khan, A.A.; Ahmad, R.; Alanazi, A.M.; Alsaif, N.; Abdullah, M.; Wani, T.A.; Bhat, M.A. Determination of anticancer potential of a novel pharmacoloFgically active thiosemicarbazone derivative against colorectal cancer cell lines. *Saudi Pharmaceutical Journal* **2022**, *30*(6), 815-824. https://doi.org/10.1016/j.jsps.2022.03.011.
63. Hopkins, A.L.; Keseri, G.M.; Leeson, P.D.; Rees, D.C.; Reynolds, C.H. The role of ligand efficiency metrics in drug discovery. *Nature reviews Drug discovery* **2014**, *13*(2), 105-121. https://doi.org/10.1038/nrd4163.
64. Jabeen, I.; Pleban, K.; Rinner, U.; Chiba, P.; Ecker, G. F. Structure–Activity Relationships, Ligand Efficiency, and Lipophilic Efficiency Profiles of Benzophenone-Type Inhibitors of the Multidrug Transporter P-Glycoprotein. *J. Med. Chem*. 2012, *55* (7), 3261–3273. https://doi.org/10.1021/jm201705f.
65. Leeson, P.D.; Springthorpe, B. The influence of drug-like concepts on decision-making in medicinal chemistry. *Nature reviews Drug discovery* **2007**, *6*(11), 881-890. https://doi.org/10.1038/nrd2445.
66. Ryckmans, T.; Edwards, M.P.; Horne, V.A.; Correia, A.M.; Owen, D.R.; Thompson, L.R.; Tran, I.; Tutt, M.F.; Young, T. Rapid Assessment of a Novel Series of Selective CB2 Agonists Using Parallel Synthesis Protocols: A Lipophilic Efficiency (LipE) Analysis. *Bioorganic & Medicinal Chemistry Letters* **2009**, *19*(15), 4406–4409. https://doi.org/10.1016/j.bmcl.2009.05.062.